THE ASTROPHYSICAL JOURNAL, 170:25–52, 1971 November 15

RADIAL VELOCITIES AND LINE STRENGTHS OF EMISSION LINES ACROSS THE NUCLEAR DISK OF M31

VERA C. RUBIN* AND W. KENT FORD, JR.*
Department of Terrestrial Magnetism, Carnegie Institution of Washington
Received 1971 May 28

ABSTRACT

Image-tube spectra have been obtained at sixteen position angles across the nuclear bulge of M31, at a dispersion of 28 Å mm^{-1}. Emission lines of Hα, [N II] $\lambda\lambda$6548 and 6583, [S II] $\lambda\lambda$6717 and 6731, He I λ5876, and [O III] λ5007 are observed. From the measured line-of-sight velocities of the excited gas across the inner 400 pc, we obtain the following model. Gas is concentrated in a very thin rotating disk with rotational velocities of the gas increasing to V = 200 km s^{-1}; the rotation is not axially symmetric. Expansion motions as large as 100 km s^{-1} exist in position angles 68°–118° and 248°–278°, but less than 0.01 $\mathfrak{M}_\odot$ $year^{-1}$ is leaving the R = 400 pc region Excess positive velocities observed in one quadrant are correlated with positions of absorbing clouds near the nucleus of M31, and may indicate infalling motions of low lying clouds Extreme density fluctuations are present; the total mass of ionized gas to R = 400 pc is probably less than 10^5 $\mathfrak{M}_\odot$. Over this region the average surface brightness is S = 0 2 × 10^{-5} ergs cm^{-2} s^{-1} $sterad^{-1}$ in Hα, and twice this in [N II] λ6583

I. INTRODUCTION

In 1899, Scheiner (1899) published an account "On the Spectrum of the Great Nebula in Andromeda." After noting the similarity of the continuum and the absorption-line spectrum to that of the Sun, he concluded, "No traces of bright nebular lines are present, so the interstellar space in the Andromeda Nebula, just as in our stellar system, is not appreciably occupied by gaseous matter." Emission lines were detected in M31 40 years later by Babcock (1939) in regions identified by Mayall as emission nebulosities along the spiral arms. Babcock also suspected the presence of the [O II] λ3727 doublet in emission close to the nucleus, where no H II regions are found. This suspicion was confirmed by Münch (1960, 1962), who observed the [O II] lines in emission along the major and minor axes close to the nucleus. More recently, Rubin and Ford (1970 [hereafter called Paper I], especially Fig. 5) detected a narrow [N II] λ6583 emission line extending across the nuclear bulge about 4 kpc in various position angles. Because emission lines in the nuclear bulge must contain valuable information concerning the physics and dynamics of excited gas in this region, we have extended these observations.

II. OBSERVATIONS

High-dispersion spectra (28 Å mm^{-1}) of the nuclear bulge of M31 have been obtained at 16 position angles. The spectra were taken with an RCA C33011 cascade-type image intensifier on the DTM image-tube spectrograph attached to the 84-inch Kitt Peak reflector and the 72-inch Perkins telescope of the Ohio State and Ohio Wesleyan Universities at Lowell Observatory. The spectra extend from 4500 through 7500 Å, and are recorded on baked IIa-O plates. For all plates, guiding is done on an offset star to ensure spatial resolution perpendicular to the dispersion. It is normally difficult to detect weak narrow emission lines in the nuclear bulge, because the background continuum from the integrated starlight is very high. However, at higher dispersions and with longer ex-

* Visiting Astronomer at Lowell Observatory, and at Kitt Peak National Observatory, which is operated by the Association of Universities for Research in Astronomy, Inc., under contract with the National Science Foundation.

posures these weaker lines can be seen above the continuum. At 28 Å mm^{-1}, we have detected emission lines of Hα, [N II] $\lambda\lambda$6548 and 6583, [S II] $\lambda\lambda$6717 and 6731, and [O III] λ5007. The He I line λ5876 is located on the wing of the wide Na D absorption lines, so it is difficult to detect with certainty. It is probably present on two plates which include this wavelength region. Because exposure times as long as 6 hours are required, we have had to limit our spatial coverage to the region within $R = 400$ pc of the nucleus, although we detect excited gas to much larger R. Along the major axis of M31, $60'' = 200$ pc for an adopted distance of 690 kpc.

Lallemand, Duchesne, and Walker (1960) determined rotational velocities in the inner 4″.2 (14 pc) of M31, from absorption line measures. In Paper I, we presented velocities of the excited gas along the NE major axis only, from the nucleus out to $R = 8'$ (1600 pc) obtained from the [N II] λ6583 line. Thus the observations we are now reporting represent a more detailed study of a small region covered in Paper I.

Table 1 is a record of the plate material. The position angle of the spectrograph slit on the sky is measured north through east, radially from the nucleus of M31. The corresponding position angle θ in the plane of M31 is listed in the final column; an inclination of $\xi = 77°$ is adopted. To simplify the tabulation, some plates are listed twice in Table 1, in cases where the spectrum was obtained with the nucleus centered on the slit and regions with P.A. $= \theta$ and $\theta + 180°$ were both recorded. The resolution on the plates is better than 1.5 Å for plates at 28 Å mm^{-1}. The scale perpendicular to the dispersion is $35''\ \text{mm}^{-1}$ on Kitt Peak spectra, and $42''\ \text{mm}^{-1}$ on Lowell spectra, which corresponds to a resolution of about 6 pc along the major axis of M31.

Representative spectra are reproduced in Figure 1 (Plate 1). The emission lines in the nuclear bulge are very asymmetrical across the nucleus. Generally, the lines are no broader than nightsky lines of comparable intensity, implying a velocity dispersion of 70 km s^{-1} or less. However, there are regions where the line of sight crosses a dust lane, and here the lines become broader. This will be discussed in greater detail below.

Measures of the emission lines were made on a Mann two-coordinate measuring machine with punched card output, and velocities were determined by means of conventional procedures. The resulting line-of-sight velocities, reduced to the Sun, are tabulated in Table 2 as a function of distance from the nucleus in seconds of arc on the plane of the sky. These measured velocities are plotted in Figure 2, for each position angle. At each position angle, velocities measured from all lines of all plates are plotted together. The scatter on the plots is an indication of the uncertainty of the velocities, which is probably less than 50 km s^{-1} in most cases, but higher for some weak exposures. To convert distance on the sky to distance in M31 for a given position angle, conversion factors are given in the Appendix.

Three plates (1962, 1965, 1967) were taken with the slit not radial from the nucleus, but parallel to the minor axis, displaced 60″ (NE or SW) from the nucleus. These locations were chosen so as to pass through the velocity maximum observed in P.A. 45° (7° to the NE major axis). For these spectra, the location of the slit was carefully positioned by the presence of a star 60″ from the nucleus along the SW major axis. The line-of-sight velocities from these plates are plotted in Figure 3. Where these slit positions intersect positions observed with the slit radial from the nucleus, excellent agreement among the velocities is seen. These additional velocities are plotted as triangles in Figure 2. Finally, the velocities along the major and minor axes observed by Münch (1960, 1962) from the [O II] lines are also plotted; the agreement is excellent.

In addition to the velocity information contained in the spectra, there is also information concerning the relative line strengths and line widths, which we shall discuss below.

III. THE VELOCITY FIELD OF THE EXCITED GAS

The emission lines observed across the nuclear bulge of M31 are generally no broader than the nightsky lines of comparable intensity. Hence, the velocity dispersion along a

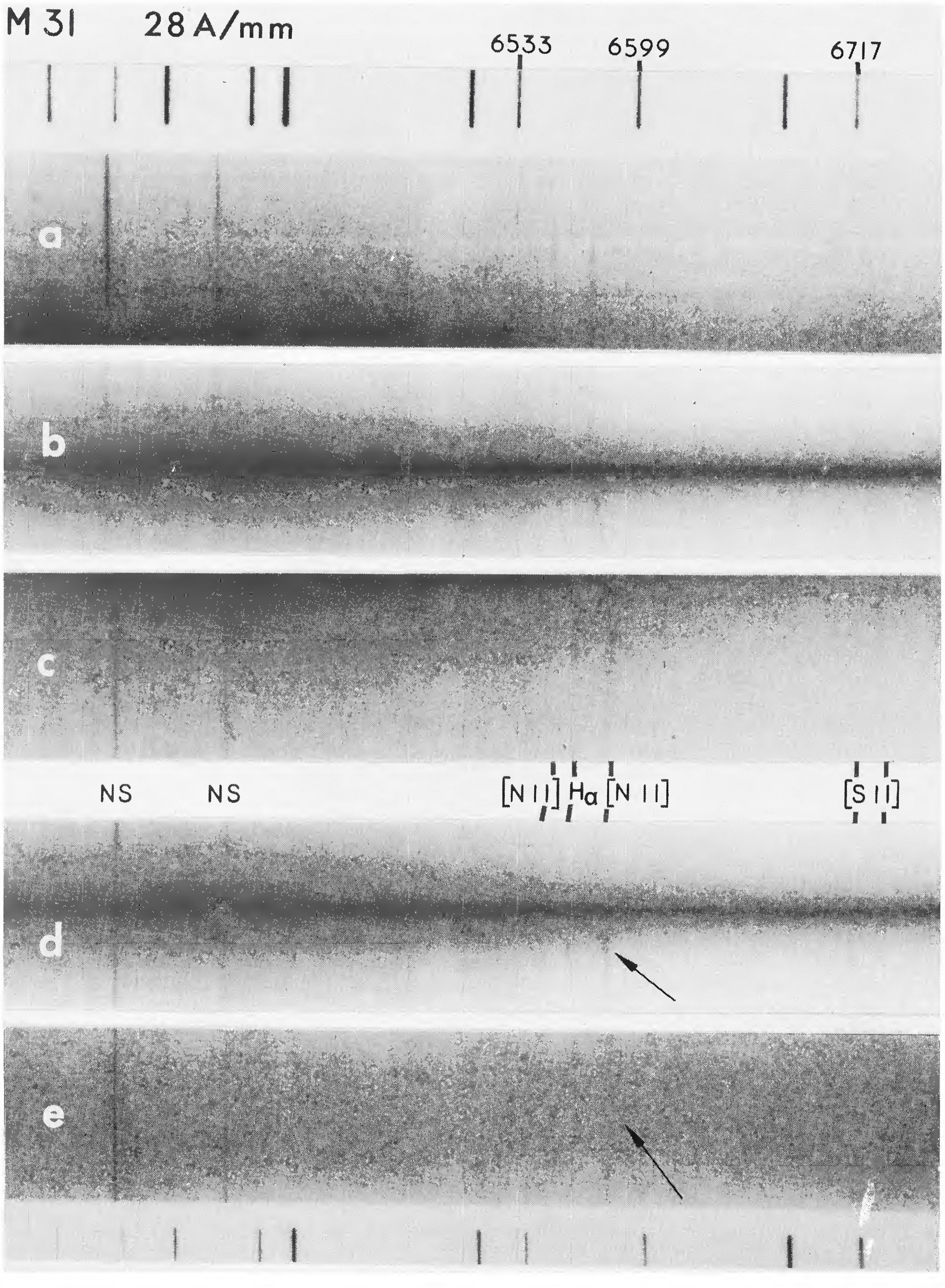

FIG. 1.—Image-tube spectra across nuclear bulge of M31, showing emission lines of [N II] λ6548, Hα, [N II] λ6583, and [S II] λλ6717, 6731. Original dispersion 28 Å mm^{-1}, baked IIa-O plates, 84-inch telescope. (*a*) Plate 1785, P.A. 218°, exposure 5^{h}46^{m}. (*b*) Plate 1786, P.A. 218° and 38°, exposure 3^{h}51^{m}. (*c*) Plate 1782, P.A. 38°, exposure 5^{h}43^{m}. (Spectra *a* and *c* overlap slightly in position with spectrum *b*.) (*d*) Plate 1798, P.A. 68°, exposure 4^{h}53^{m}. (*e*) Plate 1962, perpendicular to major axis, crossing 60″ NE of nucleus, exposure 5^{h}39^{m}.

Note that at positions where emission lines broaden (especially on *d* and *e* at location of arrows), there is a horizontal absorption lane, as light from the background integrated starlight is absorbed.

RUBIN AND FORD (*see* page 26)

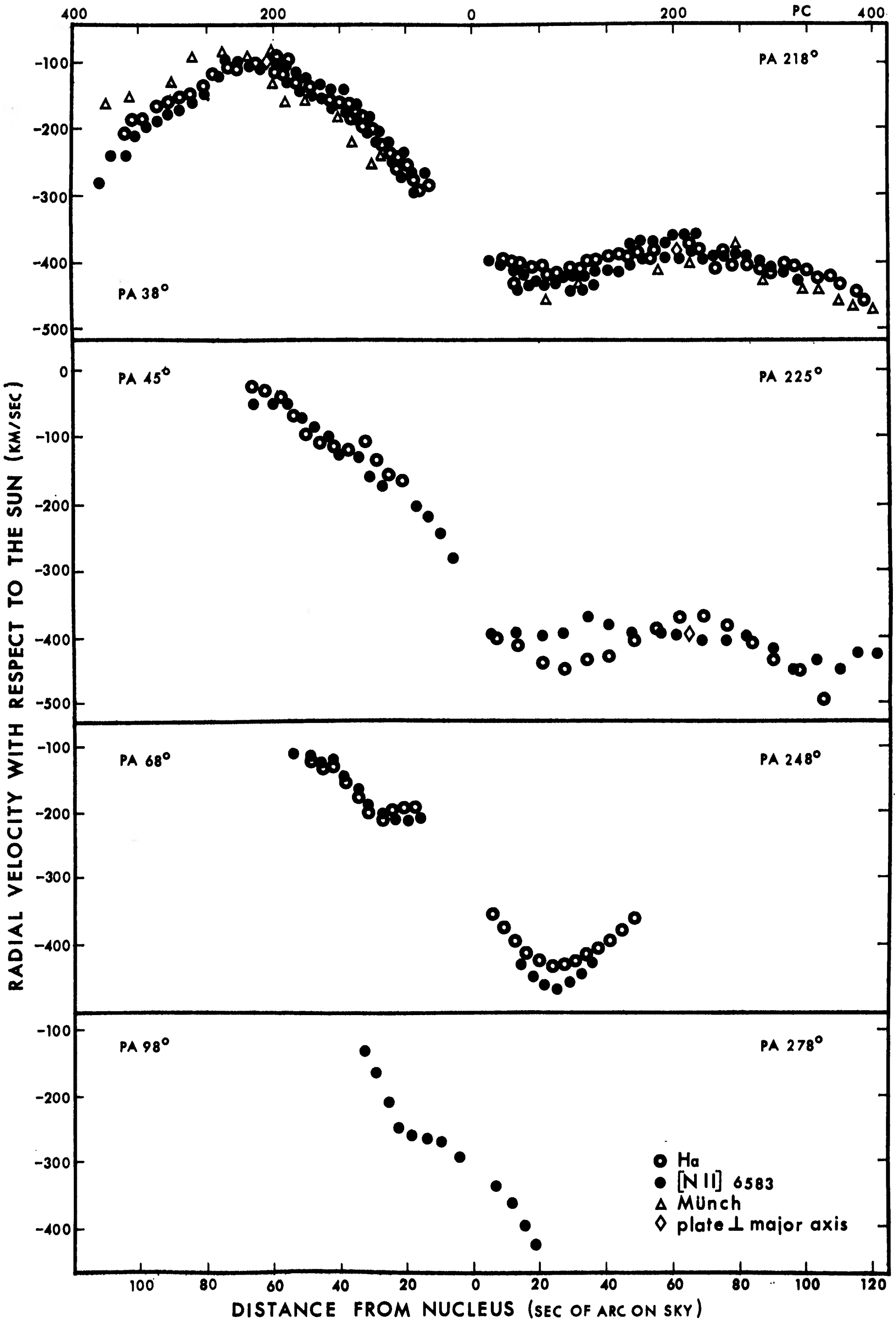

FIG. 2*a*.—Observed radial velocities reduced to the Sun, as a function of distance from nucleus of M31, for 8 position angles. For all position angles, slit radial from nucleus. Scale in parsecs refers to major axis only.

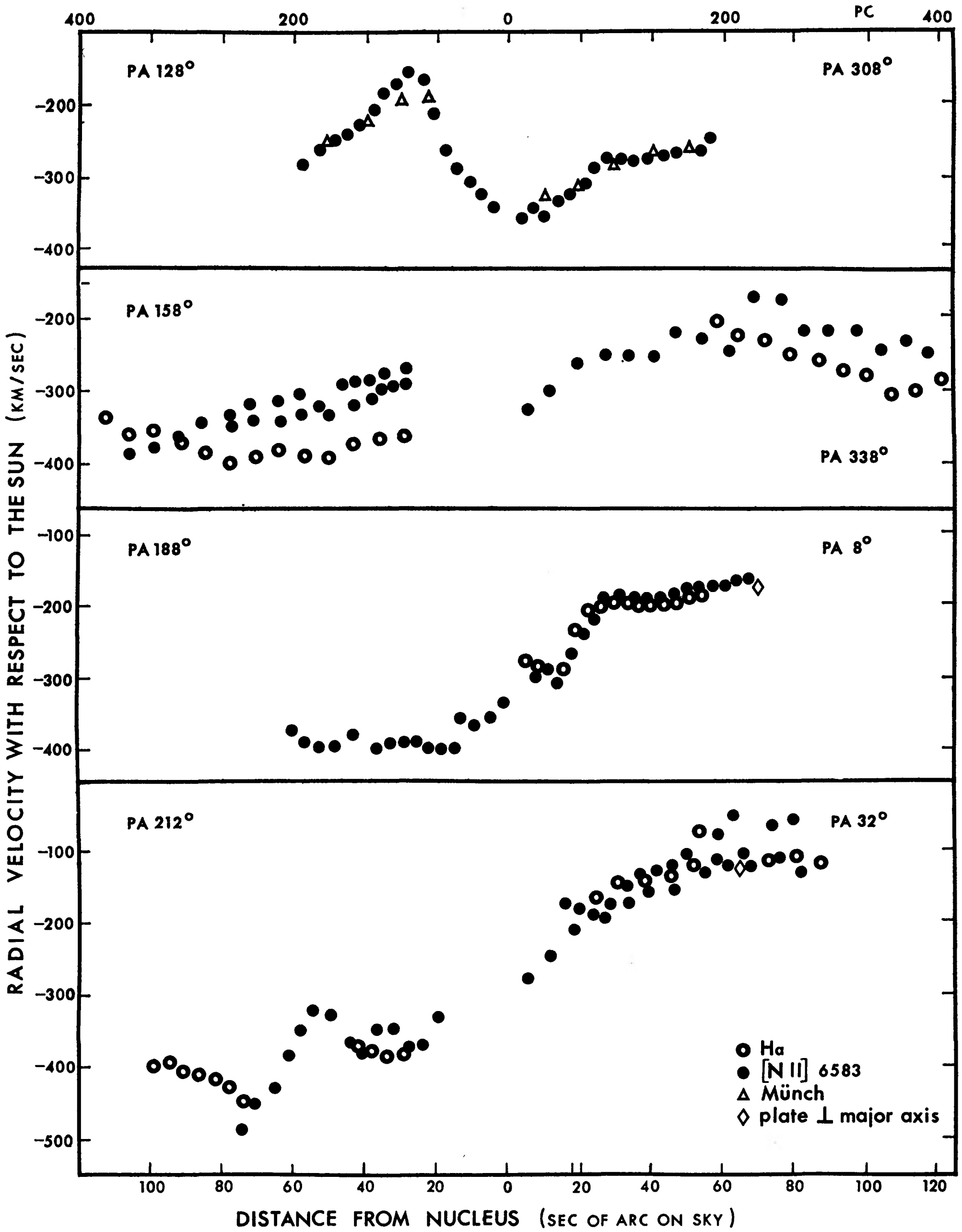

FIG. 2*b*.—Same as Fig. 2*a*

line of sight is less than 70 km s^{-1}. For a gas layer of thickness D, our line of sight crosses a distance $D' = D \sec \xi = 4D$. Because velocity variations as great as 100 km s^{-1} exist in the nuclear gas in regions separated only by 100 pc, we require that D' be of the order of 100 pc. The gas layer is thus extremely thin and of the order of 25 pc thick. In the models which follow, we assume that we are observing an optically thin gas located in a very thin layer, that the disk is coplanar with the principal plane of M31, and inclined 77° to the line of sight. Later models will consider motions out of the plane. We have not considered a model in which the gas is optically thick and we are seeing only the

TABLE 1

HIGH-DISPERSION SPECTRA ACROSS THE NUCLEAR BULGE OF M31

Plate	Position angle on sky	Dispersion A/mm	Date	Exposure	Extent of emission	Position angle in plane of M31
1782 KP	38°	28	1969 Oct. 8	5^h43^m	14"-112"	0°
1786 KP	38°	28	1969 Oct 9	3^h51^m	9"- 59"	0°
1825 L	45°	66	1969 Nov. 13	1^h15^m	5"- 67"	29°
1798 KP	68°	28	1969 Oct 11	4^h53^m	17"- 53"	69°
1802 L	98°	66	1969 Oct 13	1^h04^m	4"- 32"	83°
1794 KP	128°	28	1969 Oct 10	3^h45^m	3"- 56"	90°
1805 L	158°	66	1967 Oct. 13	45^m	28"- 78"	97°
1804 L	158°	66	1967 Oct 13	44^m	33"- 37"	97°
1963 KP	158°	28	1970 Oct 27	3^h18^m	29"-113"	97°
1799 KP	188°	28	1969 Oct 11	4^h53^m	6"- 60"	111°
1830 L	212°	66	1969 Nov. 14	2^h00^m	7"- 99"	154°
1785 KP	218°	28	1969 Oct. 9	5^h46^m	14"-140"	180°
1786 KP	218°	28	1969 Oct 9	3^h51^m	5"- 68"	180°
1987 KP	225°	28	1970 Oct. 25	4^h30^m	6"-125"	209°
1798 KP	248°	28	1969 Oct. 11	4^h53^m	6"- 49"	249°
1802 L	278°	66	1969 Oct. 13	1^h04^m	7"- 19"	263°
1794 KP	308°	28	1969 Oct 10	3^h45^m	4"- 56"	270°
1959 KP	338°	28	1970 Oct 26	4^h21^m	6"-142"	277°
1799 KP	8°	28	1969 Oct 11	4^h53^m	5"- 67"	291°
1827 L	32°	66	1969 Nov 13	1^h38^m	17"- 80"	334°
1969 KP	32°	28	1970 Oct. 29	5^h00^m	6"- 88"	334°
1962* KP	128°	28	1970 Oct 27	5^h39^m	68"NW-65"SE	
1967* KP	128°	28	1970 Oct. 28	2^h33^m	48 NW-71 SE	
1965* KP	128°	28	1970 Oct. 28	5^h33^m	19 NW-19 SE	
1824* L	45°	66	1969 Nov 13	1^h20^m	52 NE-62"NE	

*Plate not radial from nucleus

1962, 1967 Crossing major axis 60" NE of nucleus

1965 Crossing major axis 60" SW of nucleus

1824 Passing through star W of nucleus

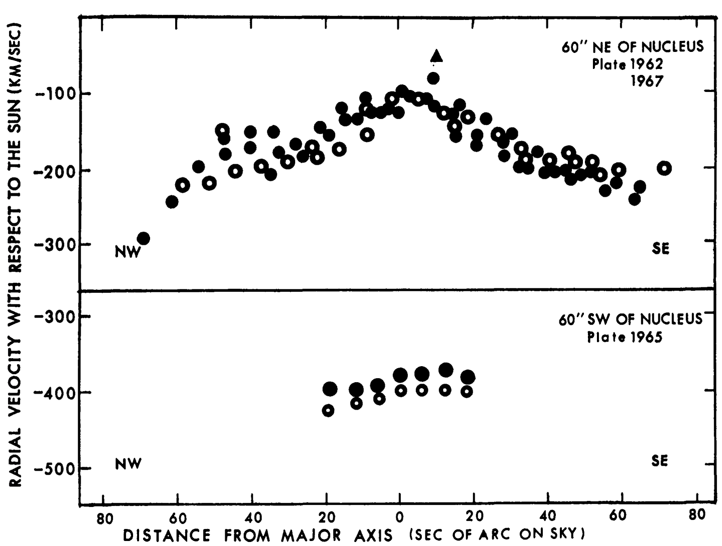

FIG. 3.—Observed radial velocities reduced to the Sun, as a function of distance from the major axis, for 2 slit locations Slit position angle 128°, i.e., slit perpendicular to major axis Symbols as in Fig 2.

TABLE 2

EMISSION-LINE VELOCITIES IN THE NUCLEAR BULGE OF M31

λ	R (arc sec)	V (km s^{-1})
Plate 1782, PA 38°		
Hα	14	-311
	17	-280
	21	-257
	24	-238
	28	-207
	31	-196
	34	-188
	38	-164
	42	-158
	45	-152
	48	-153
	52	-130
	56	-119
	59	-113
	63	-104
	66	-103
	70	-104
	73	-107
	76	-119
	80	-137
	84	-150
	87	-156
	91	-160
	94	-168
	98	-185
	101	-183
	104	-204
[N II]	17	-298
	21	-275
	24	-248
	28	-217
	31	-206
	34	-186
	38	-181
	42	-171
	45	-156
	48	-154
	52	-146
	56	-131
	59	-118
	63	-109
	66	-108
	70	- 97
	73	-100
	76	-118
	80	-151
	84	-160
	87	-169
	91	-179
	94	-183
	98	-195
	101	-215
	104	-233
	108	-237
	112	-276
Plate 1786, PA 38°		
Hα	9	-306
	12	-288
	16	-292
	20	-260
	23	-247
	26	-223
	30	-204
	34	-184
	37	-174
	40	-160
	44	-149
	48	-134
	51	-118
	54	- 98
	58	- 90
[N II]	14	-266
	18	-264
	21	-236
	25	-221
	28	-208
	32	-186
	35	-161
	38	-140
	42	-140
	46	-134
	49	-124
	53	-116
	56	-105
	59	-108
Plate 1825, PA 45°		
Hα	20	-169
	24	-158
	28	-133
	32	-108
	36	-124
	41	-117
	45	-113
	49	- 97
	53	- 65
	57	- 41
	62	- 34
	67	- 28
[N II]	5	-292
	9	-257
	13	-227
	17	-215
	22	-180
	26	-181
	30	-171
	34	-137
	39	-126
	43	-109
	47	- 92
	51	- 71
	55	- 57
	59	- 53
	65	- 54
Plate 1798, PA 68°		
Hα	17	-197
	20	-191
	24	-204
	27	-210
	31	-205
	34	-177
	38	-158
	42	-133
[N II]	17	-212
	20	-216
	24	-212
	27	-211
	31	-191
	34	-175
	38	-150
	42	-130
	45	-128
	48	-124
	53	-116
Plate 1802, PA 98°		
[N II]	4	-287

TABLE 2—*Continued*

λ	R (arc sec)	V (km s^{-1})
	8	-265
	13	-262
	17	-258
	21	-248
	25	-213
	29	-161
	32	-129
Plate 1794, PA 128°		
	3	-344
	7	-327
	10	-315
	14	-290
	17	-265
	21	-217
	24	-169
	28	-162
	31	-177
	35	-181
	38	-208
	42	-235
	45	-244
	49	-250
	52	-262
	56	-286
Plate 1805, PA 158°		
[N II]	28	-273
	31	-296
	35	-280
	39	-290
	43	-288
	47	-291
	52	-328
	58	-309
	64	-313
	69	-274
	72	-323
	78	-351
Plate 1804, PA 158°		
[N II]	33	-301
	37	-316
Plate 1963, PA 158°		
Hα	29	-366
	36	-367
	43	-376
	50	-396
	57	-395
	64	-385
	71	-395

λ	R (arc sec)	V (km s^{-1})
	78	-402
	85	-389
	92	-370
	99	-372
	106	-367
	113	-339
[N II]	36	-303
	43	-322
	50	-333
	57	-334
	64	-346
	71	-341
	78	-337
	85	-344
	92	-363
	99	-380
	106	-388
Plate 1799, PA 188°		
[N II]	6	-362
	9	-370
	13	-385
	16	-397
	19	-400
	23	-394
	26	-390
	30	-389
	33	-393
	37	-397
	43	-381
	49	-395
	53	-399
	56	-388
	60	-374
Plate 1830, PA 212°		
Hα	29	-383
	33	-382
	38	-378
	42	-367
	69	-450
	73	-448
	78	-427
	82	-412
	86	-409
	90	-409
	94	-393
	99	-398
[N II]	7	-210
	11	-229
	15	-257

λ	R (arc sec)	V (km s^{-1})
	19	-328
	23	-370
	28	-371
	32	-345
	36	-348
	40	-384
	44	-364
	49	-323
	53	-316
	57	-346
	61	-383
	65	-426
	70	-449
	74	-487
Plate 1785, PA 218°		
Hα	14	-440
	17	-439
	20	-429
	24	-422
	27	-415
	31	-415
	34	-402
	37	-398
	41	-395
	45	-388
	48	-396
	52	-393
	55	-391
	59	-382
	62	-388
	66	-389
	69	-394
	73	-410
	76	-388
	79	-404
	83	-402
	87	-419
	90	-416
	94	-412
	97	-406
	101	-414
	104	-424
	108	-424
	111	-432
	115	-445
	118	-457
	122	-474
	125	-470
	129	-479

TABLE 2—*Continued*

λ	R (arc sec)	V (km s^{-1})
	132	-479
	136	-493
	140	-492
[N II]	14	-446
	17	-435
	20	-435
	24	-434
	27	-427
	31	-423
	35	-424
	38	-416
	42	-415
	45	-416
	48	-407
	52	-404
	56	-398
	59	-396
	62	-400
	66	-388
	70	-396
	73	-394
	76	-386
	80	-391
	84	-398
	87	-405
	91	-411
	94	-418
	98	-434
Plate 1786, PA 218°		
Hα	8	-398
	12	-396
	15	-406
	19	-409
	22	-407
	26	-416
	29	-424
	33	-412
	36	-396
	47	-373
	50	-389
	54	-396
	57	-378
	61	-369
	64	-372
	68	-383
[N II]	5	-401
	9	-407
	12	-419

λ	R (arc sec)	V (km s^{-1})
	16	-422
	19	-432
	23	-436
	26	-444
	30	-449
	33	-447
	37	-439
	47	-375
	51	-369
	54	-371
	58	-374
	61	-360
	65	-363
	68	-358
Plate 1957, PA 225°		
Hα	7	-407
	14	-420
	21	-443
	28	-456
	35	-437
	42	-432
	49	-413
	56	-398
	63	-377
	70	-375
	77	-393
	84	-412
	91	-436
	98	-456
	105	-498
[N II]	6	-398
	13	-396
	20	-403
	27	-396
	34	-380
	41	-388
	48	-396
	55	-399
	62	-409
	69	-411
	76	-415
	83	-413
	90	-422
	97	-457
	104	-443
	111	-455
	118	-426
	125	-429

λ	R (arc sec)	V (km s^{-1})
Plate 1798, PA 248°		
Hα	6	-359
	10	-381
	13	-400
	16	-414
	20	-427
	24	-436
	27	-433
	31	-433
	34	-421
	38	-413
	41	-402
	45	-388
	49	-369
[N II]	15	-431
	18	-453
	22	-464
	25	-470
	29	-462
	32	-449
	36	-431
	39	-417
Plate 1802, PA 278°		
[N II]	7	-335
	12	-361
	16	-395
	19	-415
Plate 1794, PA 308°		
[N II]	4	-362
	7	-349
	10	-358
	14	-339
	18	-325
	21	-314
	24	-291
	28	-277
	32	-279
	35	-286
	39	-280
	42	-273
	46	-270
	49	-270
	53	-267
	56	-249
Plate 1959, PA 338°		
Hα	58	-209
	65	-228
	72	-234
	79	-258
	86	-284

TABLE 2—*Continued*

λ	R (arc sec)	V (km s^{-1})
	93	-275
	100	-285
	107	-310
	114	-309
	121	-285
	128	-316
	135	-287
	142	-245
[N II]	6	-327
	13	-304
	20	-265
	27	-251
	34	-256
	41	-256
	48	-223
	55	-234
	62	-251
	69	-171
	76	-177
	83	-224
	90	-225
	97	-225
	104	-248
	111	-239
	118	-251
	125	-241
	132	-232
	139	-229
Plate 1799, PA 8°		
Hα	5	-274
	8	-284
	12	-295
	15	-290
	19	-230
	22	-206
	26	-200
	29	-194
	33	-197
	36	-200
	40	-200
	43	-196
	47	-200
	50	-189
	54	-189
[N II]	7	-300
	11	-291
	14	-309
	18	-270
	21	-236

λ	R (arc sec)	V (km s^{-1})
	25	-215
	28	-191
	32	-188
	35	-190
	39	-196
	42	-192
	46	-184
	49	-178
	53	-178
	56	-177
	60	-176
	63	-167
	67	-167
Plate 1827, PA 32°		
[N II]	17	-169
	21	-180
	25	-185
	29	-174
	33	-147
	38	-128
	42	-127
	46	-118
	50	-103
	54	- 67
	59	- 74
	63	- 48
	75	- 62
	80	- 52
Plate 1969, PA 32°		
Hα	25	-165
	32	-149
	39	-139
	46	-131
	53	-121
	60	-112
	67	-108
	74	-114
	81	-109
	88	-117
[N II]	6	-274
	13	-240
	20	-206
	27	-190
	34	-165
	41	-157
	48	-150
	55	-127
	62	-120
	69	-115

λ	R (arc sec)	V (km s^{-1})
	76	-109
	83	-126
Plate 1962, PA 128° 60" NE, parallel minor axis		
Hα	-58*	-222
NW	-51	-220
	-44	-203
	-37	-197
	-30	-190
	-23	-172
	-16	-147
	- 9	-121
	- 2	-111
	+ 5	-110
	+12	-129
	+19	-131
	+26	-160
	+33	-175
	+40	-193
	+47	-193
SE	+54	-211
[N II]	-35	-207
λ6548	-28	-166
NW	-21	-148
	-14	-134
	- 7	-125
	0	-121
	+ 7	-107
	+14	-126
	+21	-158
	+28	-164
	+35	-199
	+42	-206
	+49	-209
	+56	-229
SE	+63	-244
[N II]	-68	-292
λ6583	-61	-245
NW	-54	-195
	-47	-182
	-40	-169
	-33	-177
	-26	-184
	-19	-153
	-12	-132
	- 5	-125
	+ 2	-100
	+ 9	- 77

TABLE 2—*Continued*

λ	R (arc sec)	V (km s^{-1})	λ	R (arc sec)	V (km s^{-1})	λ	R (arc sec)	V (km s^{-1})
	+16	-166		+40	-193	Plate 1965, PA 128°		
	+23	-132		+46	-181	60" SW, parallel minor		
	+30	-156		+52	-193	axis		
	+37	-179		+57	-204	Hα	-19	-423
	+44	-205		+65	-238	NW	-12	-415
	+51	-207	SE	+71	-253		- 6	-408
	+58	-222	[N II]	-47	-158		0	-399
SE	+65	-226	NW	-40	-150		+ 6	-398
Plate 1967, PA 128°				-34	-147		+12	-401
60" NE, parallel minor				-16	-118	SE	+18	-400
axis				- 9	-104	[N II]	-19	-395
Hα	-48	-148		- 3	-111	NW	-12	-396
NW	-40	-151		+ 3	-105		- 6	-393
	-34	-158		+ 9	-117		0	-378
	-28	-183		+15	-159		+ 6	-375
	-22	-188		+21	-167		+12	-369
	-16	-178		+28	-185	SE	+19	-380
	- 9	-158		+34	-197	Plate 1824, PA 45°		
	- 3	-114		+40	-202	[N II]	52†	-370
	+ 3	-100		+46	-214		56	-374
	+15	-148		+52	-240	NE	62	-397
	+22	-165		+59	-181			
	+28	-177		+65	-220			
	+34	-191	SE	+71	-239			

* For plates 1962, 1967, and 1965, not radial from the nucleus, Y = 0 corresponds to position of star, located approximately on major axis, 60" SW of nucleus.

† Y = 0 corresponds to second star W of nucleus

near edge of the gas distribution, for such a situation does not appear to be realistic. In all discussions, we refer to the excited gas only; the stellar velocities in the nuclear bulge have not been studied.

It is immediately clear from the variation of velocity shown in Figure 2 that the velocity field in the nuclear bulge is more complex than just a simple rotation. In most position angles the velocities are not symmetrical about the origin. Near the NE major axis there are steep velocity gradients, and negligible gradients on the SW side. To investigate the velocity field in more detail, we have drawn smooth curves through the observed velocities in each position angle in Figure 2, and have read values for the velocities for each 10″ on the plane of the sky. In Table 3 we list these velocities minus the central velocity; we adopt $V_{cent} = -300$ km s^{-1}. These velocities are plotted in Figure 4, where isovelocity lines have been drawn. If the velocity field arises from a rotation only, the minor axis will exhibit zero velocities, and the NE and SW regions of the galaxy will have equal but opposite velocities. The schematic diagram in the lower left of Figure 4 shows the predicted velocities for a rotating disk, viewed at an inclination of 77°.

Notable departures from a simple rotation pattern are observed. Along the minor axis where rotational components are zero, velocities as large as 130 km s^{-1} are seen.

1971ApJ...170...25R

TABLE 3

Smoothed Line-of-Sight Velocities Minus Central Velocity for Sixteen Position Angles in Nuclear Bulge of M31

R (arc sec on sky)	Position Angle on Sky 38°	45°	68°	98°	128°	158°	188°	212°	218°	225°	248°	278°	308°	338°	8°	32°
5	...	+ 10	...	+ 10	− 40	...	−50	...	−100	− 95	− 55	...	−55	−30	+ 10	+ 25
10	0*	+ 50	...	+ 30	− 15	...	−70	...	−115	−102	− 90	− 50	−50	−10	+ 5	+ 50
20	+ 42	+100	+ 85	+ 50	+ 45	...	−95	− 42	−130	−110	−142	−125	−15	+30	+ 50	+100
30	+ 82	+150	+100	+142	+130	+ 5	−92	− 75	−125	−107	−145	...	+20	+45	+105	+137
40	+128	+190	+155	...	+ 80	− 5	−95	− 70	−115	−105	−110	...	+25	+50	+105	+168
50	+160	+218	+178	...	+ 45	−15	−95	− 50	−100	−100	− 65	...	+30	+63	+120	+180
60	+188	+230	+180	...	+ 5	−25	−72	− 75	− 90	− 95	...	...	...	+70	+175	+185
70	+200	+240	...	...	...	−35	...	−150	− 95	− 97	...	...	...	+70	+135	+190
80	+178	...	...	...	...	−50	...	−122	− 97	−115	...	...	...	+65	...	+190
90	+152	...	...	...	...	−60	...	−105	−105	−138	...	...	...	+55	...	+185
100	+102	...	...	...	...	−70	...	−100	−115	−155	...	...	...	+45	...	...
110	+ 98	...	...	...	...	−75	...	...	−135	−155	...	...	...	+38	...	...
120	+190	...	...	...	...	...	...	...	−165	−140	...	...	...	+35	...	...
130	...	...	...	...	...	...	...	...	−180	...	...	...	...	+35	...	...
140	...	...	...	...	...	...	...	...	−190	...	...	...	...	+40	...	...

* In km s^{-1}, reduced to the Sun.

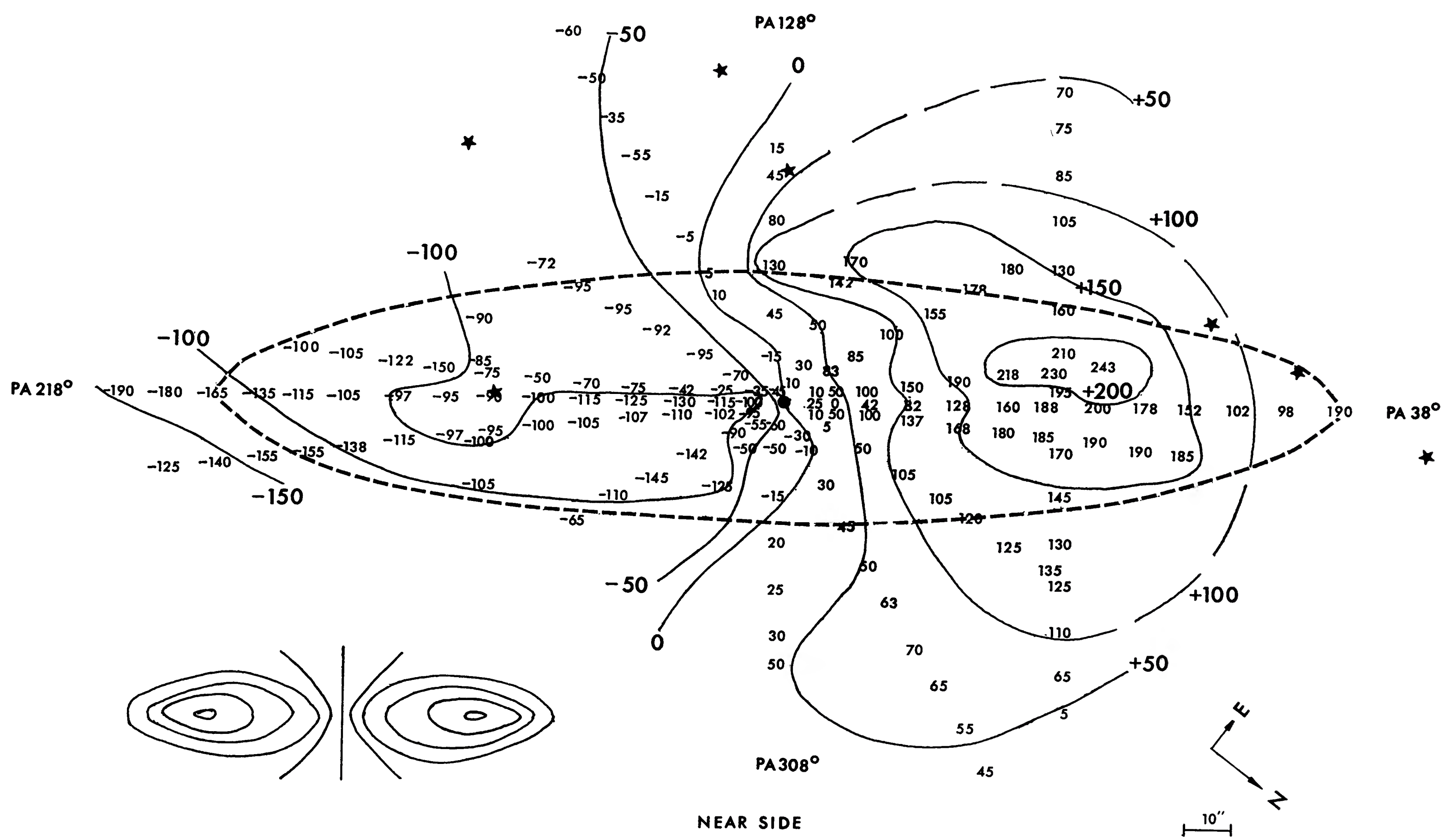

FIG. 4.—Smoothed radial velocities minus central velocity for 16 position angles, plotted each 10″ on plane of sky. Ellipse represents extent of a thin disk of 400 pc, viewed at an angle of $\xi = 77°$. Isovelocity contours are drawn. Schematic diagram in lower left indicates predicted isovelocity lines for simple rotation law.

Near the NE major axis there are steep velocity gradients, while near the SW major axis there are negligible velocity gradients. Hence, it appears that both circular and noncircular motions must be present, either in the form of motions radial from the center, motions perpendicular to the plane, or random motions of the order of 100 km s^{-1}.

To show that a major component of the observed velocities is a rotational component, we proceed as follows. Consider a point moving in the plane of M31, with nebular coordinates R, θ. The observed radial velocity is related to the circular component $V(R)$ and the expansion component $E(R)$,

$$V_{\rm obs} - V_{\rm cent} = V(R) \sin \xi \cos \theta + E(R) \sin \xi \sin \theta \, , \tag{1}$$

where $V_{\rm cent}$ is the systemic velocity of the galaxy. In the plane of the sky, the point has coordinates X directed along the major axis, and Y directed along the minor axis; $\cos \theta = X/R$, $\sin \theta = (Y \sec \xi)/R$, and $R = (X^2 + Y^2 \sec^2 \xi)^{1/2}$. The angle ξ is the angle between the line of sight and the perpendicular to the plane of the galaxy; we adopt $\xi = 77°$. If only circular motions are present in the plane of M31, then

$$V_{\rm obs} - V_{\rm cent} = V(R) \sin \xi \cos \theta \, . \tag{2}$$

If we now assume a simple rotation law for the central region of M31, then all points at a given distance from the nucleus R_1 will have circular velocity V_1. The observed velocities will vary as the cosine of the azimuthal angle θ, with the amplitude of the cosine variation, from equation (2), equal to $V_1 \sin \xi$. Velocities will be a maximum and minimum along the major axis, and will equal the central velocity along the minor axis. At a larger distance from the nucleus, $R = R_2$, the observed velocities will be a cosine function of the same phase, but of amplitude $V_2 \sin \xi$.

In Figure 5 we plot the observed velocities as a function of azimuthal angle θ for five values of R, 20″ to 60″ (in the plane of M31), as well as predicted velocities for a simple rotation law. The observed velocities rise to a maximum near the NE major axis and a minimum near the SW major axis, and in general exhibit a cosine-like dependence with θ. However, departures from the simple variation are present, notably along the SW major axis, where large negative velocities are not observed, and in P.A. 45°, where the observed velocities are larger than those observed along the major axis. From the symmetry of the curve, however, we conclude that P.A. 38° is within a few degrees of the major axis, that $V = -300$ km s^{-1} is a satisfactory choice for $V_{\rm cent}$ and that a major component of the observed velocity variation does come from the rotation of a thin disk.

As will be seen below, if we adopt a simple rotation law for the nuclear disk, residual velocities as large as 100 km s^{-1} remain. Hence, we would like to answer the question, "Is there a relatively simple patterned motion, involving rotation, radial motions, and z-motions, which seems plausible on dynamical grounds and which can account for the line-of-sight velocities, or must we be content to characterize the large departures from the rotation as large random motions?" Our choice to search for a patterned motion was made principally because (1) the departures from circular motion appear systematic from position angle to position angle over a sizable region of the nuclear disk, and (2) we wished to see just how complicated a model would be required to reproduce the observed velocities.

To examine the residual velocities, after taking account of the rotation, we have investigated several models.

Model I.—Axial symmetry in the plane of M31 was assumed and a linear rotation law was adopted, rising from $V = 0$ at $R = 0$ to $V = 200$ km s^{-1} at $R = 400$ pc. This variation approximates the velocities of the neutral hydrogen in the nuclear disk of our Galaxy. For the observed velocities across the nuclear bulge of M31, the residuals from this model are close to the residuals from Model II, and will not be discussed in detail.

Model II.—Axial symmetry was assumed, and a rotation curve was formed from the

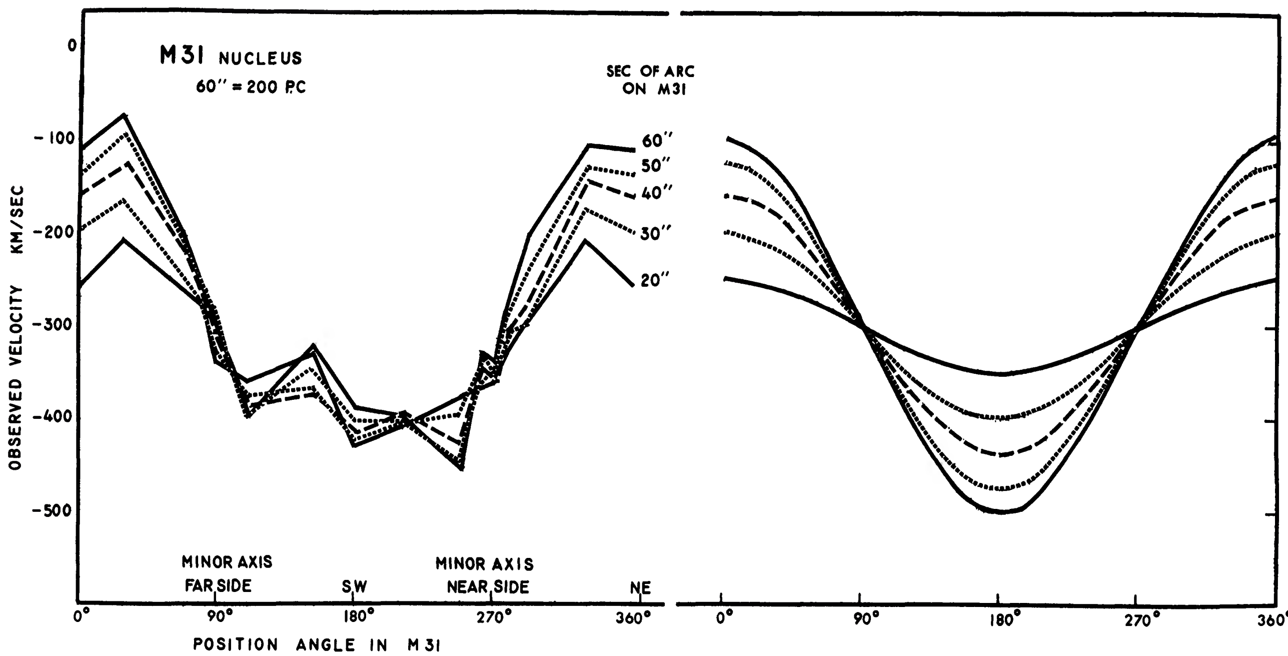

FIG. 5.—*Left*, observed radial velocities at fixed distances from nucleus of M31, as a function of azimuthal angle in plane of M31. *Right*, predicted radial velocities at fixed distances from nucleus of M31, as a function of azimuthal angle in plane of M31, for simple rotation law.

mean velocities observed along the NE and the SW major axes in the nuclear bulge of M31. For each observed position angle, and for each 10″ on the plane of the sky, the line-of-sight velocity predicted by the model was calculated, and residuals from the observed velocities were formed. The residuals are not distributed at random, but large positive residuals exist over the quadrant P.A. 45°–128° and large negative residuals ~180° away in P.A. 248°. Altering the choice of the position angle of the major axis from 38° toward 68° does not decrease the residuals overall, for then the residuals near P.A. 8° and 188° become large. The algebraic sense of the residuals is such that matter moving out from the nucleus along two axes 180° apart will produce the observed velocities. Thus, we are led to consider a model in which there are both rotational and radial motions in the plane.

Model III.—Both Models I and II are axisymmetric; i.e., there is azimuthal symmetry in the plane of M31. For Model III we retain the rotation law from Model II, but postulate nonaxisymmetric motions radial from the center of M31. From the residual velocities of Model II, we calculate the expansion velocities which, when combined with the adopted rotation, will reproduce the observations. Thus the rotational velocities of the earlier model now become the tangential components of a two-component velocity. In what follows below, we shall use the phrase "rotation of the gas" to mean the tangential component of the motion.

For the three position angles 68°, 98°, and 128°, i.e., position angles on the far side of the galaxy, a single expression $E_1(R)$ for the expansion velocity as a function of distance from the nucleus will reproduce well the residual velocities in these position angles. The expansion velocities $E_1(R)$ increase from $V = 0$ at $R = 0$ to $V = 120$ km s^{-1} at $R =$ 400 pc. In position angles ~180° from these, P.A. 248° and 278°, a similar, but not identical, expansion $E_2(R)$ which rises slightly more steeply than $E_1(R)$ will reproduce the residuals in these position angles. Values of $E_1(R)$ and $E_2(R)$ are listed in Table 4. This expansion radial from the nucleus in two position angles about 180° apart is an

TABLE 4

ROTATIONAL VELOCITIES FOR MODELS II, III, AND IV AND EXPANSION VELOCITIES FOR MODELS III AND IV

R (arc sec in M31)	R (pc in M31)	$V(R)$ (km s^{-1})	$E_1(R)$* (km s^{-1})	$E_2(R)$† (km s^{-1})	$E_3(R)$‡ (km s^{-1})
0.......	0	0	0	0	0
10.......	33	58	+ 2	+ 25	+21
20.......	67	86	+ 5	+ 39	+21
30.......	100	105	+ 9	+ 50	+16
40.......	133	122	+ 15	+ 62	+10
50.......	167	132	+ 18	+ 78	+ 2
60.......	200	141	+ 24	+ 86	− 8
70.......	233	145	+ 31	+ 94	−18
80.......	267	138	+ 47	+100	−25
90.......	300	124	+ 70	+ 93	−30
100.......	333	109	+ 91	+ 76	−33
110.......	367	119	+107	+ 46	−33
120.......	400	178	+120	+ 16	−32

* P.A. 68°, 98°, 128°.
† P.A. 248°, 278°.
‡ P.A. 188°, 308°, 338°, 8°.

outstanding feature of the velocity field near the nucleus; it was the component of this expansion along the minor axis (P.A. 128°) which was noted by Münch (1960, 1962).

For position angles away from the direction of the expansion axis, P.A. 188°, 308°, 338°, and 8°, the residual velocities from a rotation-only model are small, but can still be decreased with the adoption of a single expansion relation, $E_3(R)$, which includes small velocities of expansion, $R < 200$ pc and motions toward the nucleus, $R > 200$ pc. The adopted forms of V, E_1, E_2, and E_3 are listed in Table 4. To indicate the accuracy with which this model will reproduce the observed velocities, we plot in Figure 6 the observed velocities (points read from the smooth curves), the predicted velocities for Model II (rotation only), and the predicted velocities from Model III (rotation plus expansion), for all position angles away from the major axis, (except for P.A. 158°, which has almost no observed velocities for $R < 400$ pc). As can be seen from Figure 6, for position angles along the axes of streaming, the agreement of the predicted velocities with the observed velocities is satisfactory, especially when compared with the poor fit for the rotation-only model.

It is interesting to point out that from photographic photometry of M31 Lyngå (1959), using plates from the 18-inch Schmidt at Mount Palomar and the 60-inch Mount Wilson reflector, concluded that the intensity distribution in the nuclear bulge indicated the presence of a bar, for $R \leq 2'$ (400 pc), in P.A. = 85° ± 10° and P.A. 265° ± 10° or just in the region in which the radial expansion is observed.

Notwithstanding the excellence with which Model III can represent the observed velocities away from the major axis, there is still one shortcoming of the model. Along the major axis and in position angles close to the major axis, large residual velocities from Model III are observed. This is seen in Figure 7, where we plot the residual velocities from Model III on the plane of the sky for all position angles. Because expansion motions have a zero component along the major axis, we must appeal to z-motions, random motions, or relax the assumption of axisymmetry in the rotation curve, to account for the observations. These possibilities are considered in Models IV and V.

Model IV.—We retain the rotation and expansion components from Model III, and

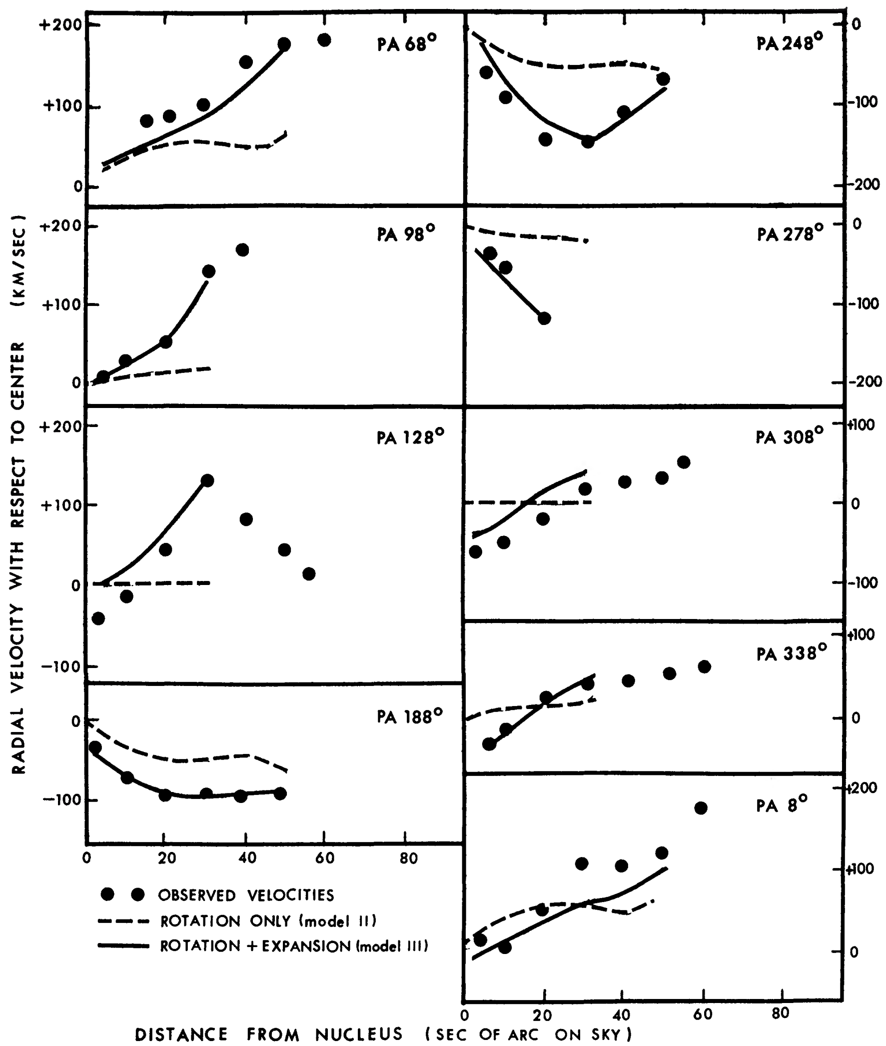

FIG. 6.—Radial velocities with respect to central velocity, as a function of distance from the nucleus, for position angles away from major axis. *Dots*, smoothed observed velocities. *Dashed lines*, predicted line-of-sight velocities, Model II (rotation only). *Solid lines*, predicted velocities, Model III (rotation plus expansion).

examine z-motions to account for the large residuals near the NE major axis. Throughout the entire velocity study, the difference between velocities on the NE and the SW parts of the major axis has been noted. Perhaps not unexpectedly, the appearance of the galaxy in the inner nuclear bulge is also very different near these two axes. We have obtained copies of several of Baade's short-exposure plates of M31 taken with the 200-inch and 100-inch telescopes, through the kindness of Henrietta Swope and William C. Miller of the Hale Observatories. One of the 200-inch plates, PH 466-B, is reproduced in Figure 8 (Plate 2). Numerous dust lanes cross the N and NE parts of the nuclear bulge on the near side of the galaxy, while much of the remaining nuclear regions of the galaxy appear free of dust (see also Johnson 1961). We have sketched the outlines of the dust patches in Figure 7, superposed on the residual velocities from Model III. In many cases the excess positive velocities occur in dust regions.

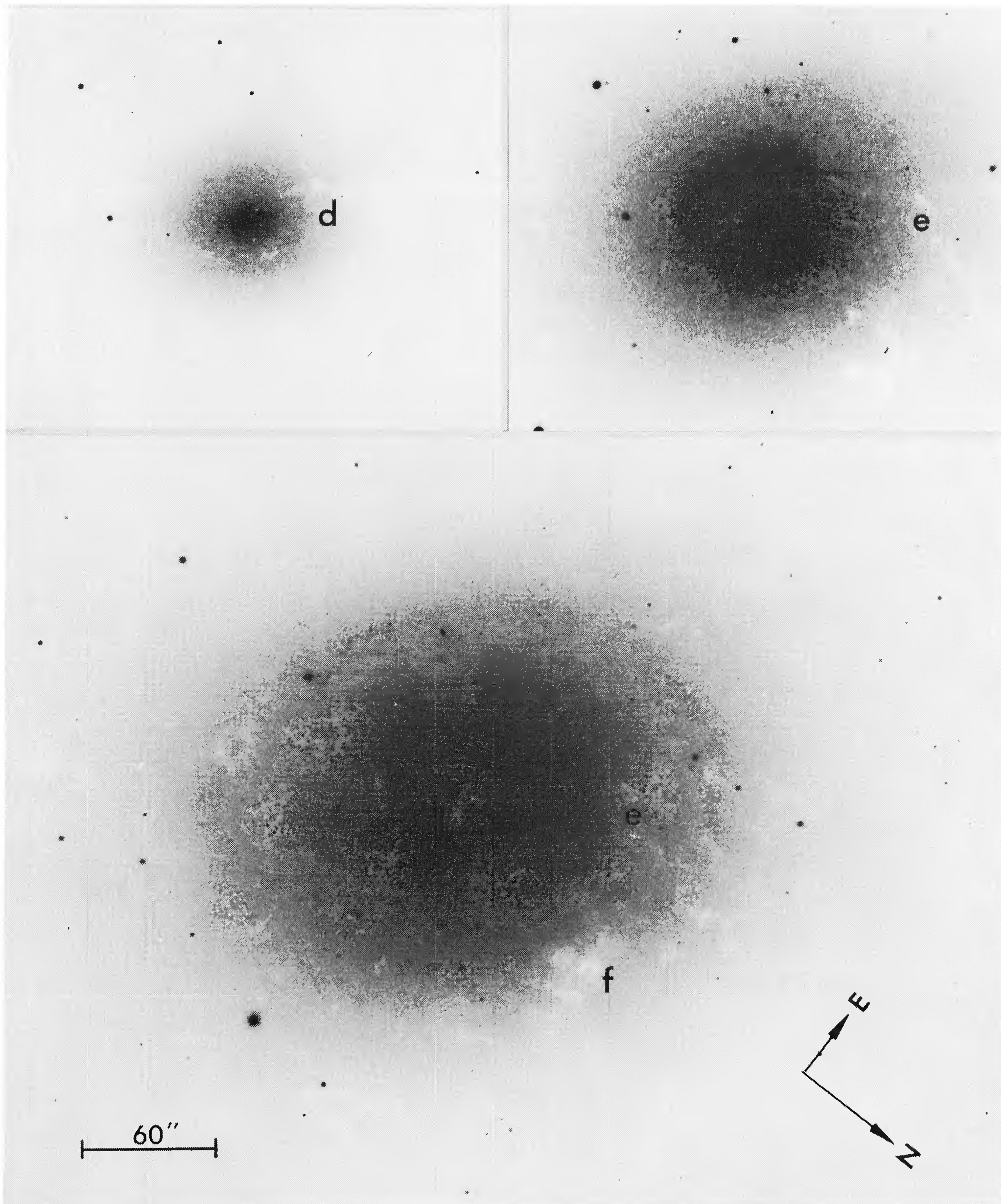

FIG. 8.—Three prints of increasing density of nuclear region of M31 from 200-inch plate by Baade, PH 466B, 1951 August 7–8, 103-O+GG1, exposure 1 minute. For all prints, scale and orientation is the same, with major axis horizontal and near edge of galaxy at bottom. Note prominent dust lanes NE of nucleus which are sketched in Fig. 7. Cloud regions marked *d* and *e* are indicated by arrows on spectra *d* and *e*, and located on Fig. 7. Photograph courtesy of the Hale Observatories.

RUBIN AND FORD (*see* page 40)

1971ApJ...170...25R

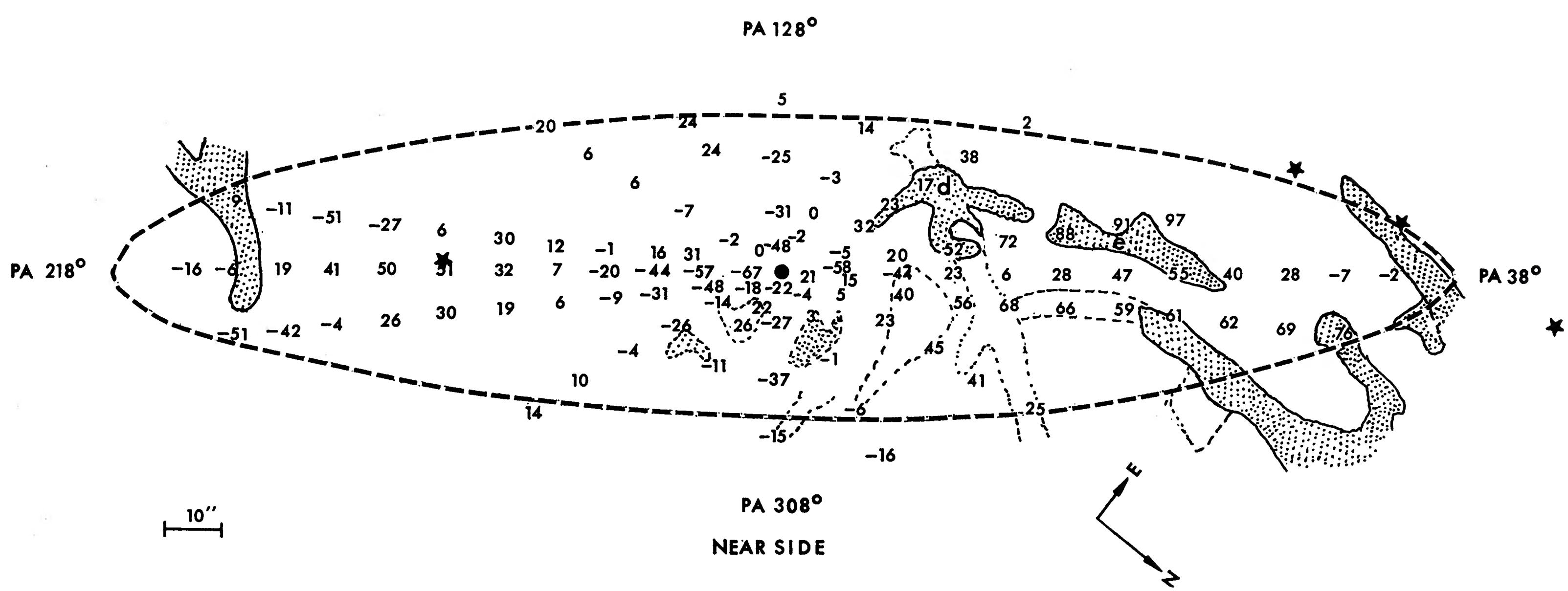

FIG. 7.—Observed velocities minus predicted velocities from Model III (rotation plus expansion), plotted on plane of sky. Dotted regions show location of principal dust clouds from Baade's plate PH 466B (see Fig. 8); dashed lines outline secondary dust clouds. Note that many large residual velocities occur at positions of dust clouds. Cloud regions marked *d* and *e* are indicated by arrows on spectra *d* and *e* (Fig. 1) and produce broadening of emission lines and absorption of the lower-lying stellar continuum. Ellipse represents extent of a thin disk with $R = 400$ pc, viewed at angle of $\xi = 77°$.

A detailed comparison of these patches with our spectra has revealed that the knots we observe on the emission lines occur always when the spectrograph slit is crossing a dust patch. Here the lines generally thicken, and there is often a velocity discontinuity. In addition, light from the background integrated starlight is absorbed, producing a horizontal absorption lane on the spectra. For example, in P.A. 45° there is a prominent dust lane marked (e) in the photograph (Fig. 8). On the spectrum there is a pronounced discontinuity in the emission line, and a very positive velocity is measured. This position corresponds to the maximum velocity residual ($v > 75$ km s^{-1}) seen in P.A. 45° in Figure 7. This observation has been confirmed by Plate 1962 taken parallel to the minor axis, displaced 60″ NE along the major axis (Fig. 1). There is a sharp velocity discontinuity, positive velocity, and absorption across the continuum at the location of dust patch (e). Another prominent dust patch (d) in P.A. 68°, $R = 30''$ (on the sky) also shows on the spectrum (Fig. 1) as an absorption in the continuum and increased intensity in the emission lines. The most pronounced discontinuity on our spectra occurs in position angle 338°, where the spectrum crosses the large dust complex marked "f" in Figure 8. A detailed comparison confirms this effect in many other locations with positive velocity residuals near the NE major axis. In the framework of Model IV, the most direct interpretation of this observation is (1) that we are looking at regions in which gas and dust are intermingled, (2) that these regions, known to be on the near side of M31, are above the plane of M31, and (3) that they are optically thick and absorbing the stellar continuum below. Because we are observing M31 only 13° to edge-on, and see these features principally on the near side of the galaxy close to the nucleus, we interpret them as low-lying clouds within 50 pc of the nuclear disk. The excess positive velocity observed in the line-of-sight velocity will then arise from an infall of these clouds to the nuclear disk. The maximum residuals have a mean value of about 60 km s^{-1}. At the angle at which we are viewing M31, we see one-fourth of any z-component; hence, the velocity would be of the order of 250 km s^{-1}, if the clouds are falling perpendicular to the plane. If the clouds are falling to the plane not along the line of $b = 90°$ (measured from the center of M31) but at some lower latitude, their velocities are correspondingly less. The lower limit to the velocity will be observed if the space motion of the clouds coincides with the line of sight; i.e., velocities of 60 km s^{-1} at angles of $b = 13°$. The only simple alternative to this model is one in which the dust patches lie in the plane of the disk of M31, and have excess positive tangential-velocity components. This does not seem likely.

While Model IV can reproduce the observed line-of-sight velocities, it ignores the differences in the velocities observed on the NE and the SW major axes. Furthermore, the velocities near the NE major axis, in P.A. 32°, 38°, and 45°, are very similar to each other, as are the observed velocities near the SW major axis, yet the NE and the SW velocities are dissimilar. In all previous models we have neglected this difference in forming a mean rotation curve. We examine this feature in Model V.

Model V.—Axial symmetry in the rotation field is not assumed, so the tangential-velocity components for the NE major axis are not identical to those for the SW major axis. With this freedom, it is possible to adopt rotational velocities for the NE major axis which are a better fit to the velocities in nearby position angles than in Model IV; however, there are still excess positive velocities, especially in P.A. 45°. Likewise, the fit can be improved with a second set of rotational velocities for the SW side, although large residuals remain in a few small regions. The major argument in favor of such a model is the similarity of the observed velocities in P.A. 32°, 38°, and 45° to each other, and the similarity of the position angles near the SW major axis to each other. Infalling motions would still exist, but with smaller velocities than those discussed above. Dynamically, neither Model IV nor Model V is long lived, and would require very special assumptions as to their origin and continued existence.

Finally, we have examined the possibility that the dynamical center of M31, on this small scale, does not correspond to the position of maximum light. No such model was successful in accounting for the observed velocities.

From all of these studies, we believe the best description of the velocity field within 400 pc of the nucleus of M31 lies somewhere between Models IV and V. The gas is concentrated to a very thin disk, rotating with velocities which rise from $V = 0$ at $R = 0$ to approximately $V = 200$ km s^{-1} at $R = 400$ pc, but strict axial symmetry is not present. Superposed on this rotation is a fairly large-scale expansion along P.A. 60°–128° and 248°–278° on the plane of the sky, corresponding to P.A. 69°–90° and P.A. 249°–263° in the plane of M31. The expansion velocity of the gas increases from $V = 0$ at $R = 0$ to $V = 100$ km s^{-1} at $R = 300$ or 400 pc. At right angles to the axis defined by the expansion, the velocities are smaller ($\sim$30 km s^{-1}) and positive, $R < 200$ pc, and negative $R > 200$ pc. The observational evidence for z-motions is less well established, but it is possible that clouds of gas and dust observed in the northern quadrant are low-lying and falling to the plane with velocities which can range up to 60–250 km s^{-1}. The mass of gas involved in this velocity field is discussed in § IV, and the model is compared with the current model of gas in the nucleus of our Galaxy in § V below.

IV. CONTINUUM AND EMISSION-LINE STRENGTHS

a) Continuum Intensity

For normal galaxies with strong emission lines in their nuclei (M51, M81), the excited gas near the nucleus often exhibits an intensity ratio I(N II)/I(Hα) larger than unity. With our observations of emission lines across the nuclear bulge of M31, we can now investigate line strengths in a weak-line galaxy. All our spectra across the nuclear bulge are calibrated with a step-wedge exposure which enables us to determine relative line intensities. In order to obtain approximate values of the absolute intensities for this limited spectral region, we have transformed our relative values through the continuum observations of the central 10″ of M31 by Peimbert (1968). Four of our spectra cross the nucleus (1786, 1794, 1798, 1799). On these plates we have traced the inner 10″ with a microphotometer, and related the measured values, corrected for extinction and reddening, as a function of wavelength, to the observations of Peimbert. Because the background continuum radiation from the stars in the nuclear bulge of M31 is decreasing very rapidly with radial distance from the nucleus, there is a steep intensity gradient on our plates over the inner 10″. Therefore, the plates were traced in several strips, with a sufficiently small scanning slit so that the intensity gradient over a single slit height was not severe. The principal difficulty in the photometry arises in choosing the continuum level. The absolute intensities determined in this manner are probably not accurate to better than about 40 percent. The internal agreement is good; in the spectral range 6548–6620 Å, the relative agreement for the intensity of the continuum radiation was within a few percent for the four plates. For a fifth plate, 1782, the overlap in position with plate 1786 was sufficient to obtain an absolute calibration for this plate as well.

The absolute continuum intensities are listed in Table 5, and plotted in Figure 9 as a function of position angle and radial distance R on the sky. The absolute continuum intensities are the fluxes received at Earth, corrected for extinction and reddening, from a rectangle 10″.5 × 1″.52 on M31. This area is defined by the spectrograph slit width (1″.52) and the scanning slit height of the microphotometer (10″.5 on the plate). The long axis is radial from the nucleus. Because the continuum arises from a nearly spherical stellar distribution, no account is taken of the inclination of the galaxy in deriving these values. On the plot, the intensity is also expressed in what are equivalent units, the surface brightness per square second of arc on M31.

TABLE 5

ABSOLUTE LINE AND CONTINUUM INTENSITIES NEAR NUCLEUS OF M31

Plate	Position angle (degrees)	R (Sec of arc on sky)	I(6548)* (10^{-13} ergs cm^{-2}sec^{-1} from area 10″.5 x 1″.5)	I(Hα)	I(6583)$^+$	I(6583)$^+$ / I(Hα)	Continuum at 6584A (10^{-13} ergs cm^{-2}sec^{-1}A^{-1} from area 10″.5 x 1″.5)	I(6583) / I(continuum)
1794	308	18 NW		0.048	0.22	4.6	0.15	1.5
1786	218	26 SW		0.040	0.066	1.6	0.14	0.47
1782	38	26 NE	0.048	0.14	0.18	1.3	0.077	2.3
1786	38	28 NE		0.049	0.18	3.7	0.12	1.5
1798	248	32 SW		0.080	0.11	1.4	0.094	1.2
1798	68	32 NE		0.11	0.16	1.5	0.092	1.7
1794	128	32 SE		0.035	0.10	2.9	0.12	0.83
1799	8	35 NE		0.036	0.094	2.6	0.10	0.94
1799	188	35 SW		0.029	0.070	2.4	0.087	0.80
1794	308	38 NW			0.061		0.068	0.90
1786	38	56 NE		0.036	0.073	2.0	0.058	1.3
1782	38	58 NE		0.071	0.13	1.7	0.058	2.2
1799	188	61 SW			0.047		0.055	0.85
1786	218	64 SW		0.020	0.033	1.6	0.055	0.60
1799	8	64 NE	0.026		0.11		0.044	2.5
1782	38	71 NE	0.042	0.035	0.080	2.3	0.045	1.8
1782	38	91 NE		0.024	0.035	1.5	0.032	1.1
1782	38	134 NE		0	0.019		0.024	0.79
Mean						2.2		1.3

* Observed flux, corrected for extinction and reddening, integrated over line width.

* 6548 = [NII] λ 6548

+ 6583 = [NII] λ 6583

Surface photometry of the nuclear region of M31 in the R-band (7000 Å) has been carried out by Sandage, Becklin, and Neugebauer (1969) with the 200-inch telescope with a circular diaphragm 7″.62 diameter, but extending only to $R = 30''$. Their results are plotted in Figure 9*a* with no adjustment between their observations and ours. Their spectral region is centered to the red of ours and over a broader spectral band, and their values are averaged over a larger spatial region. Nevertheless, in the small region of overlap the agreement is good, and increases our confidence in this coarse absolute spectrophotometry. In the region beyond $R = 30''$, where detailed photometry in the red does not exist, the surface brightness continues to drop, by a factor of 4 to $R = 90''$, and by a factor of 6 to $R = 135''$ (450 pc). Sandage *et al.* have shown that the index $V - R$ is constant with radial distance to $R = 30''$. We show in Figure 9*a* the variation of V for $30'' < R < 120''$ from Sandage *et al.* (1969) along with our values of the continuum at 6584 Å. From our observations, it appears that the surface brightness in the red may be decreasing relative to the surface brightness in the V-band, for $R > 30''$. However, more accurate photometric observations are necessary to confirm this.

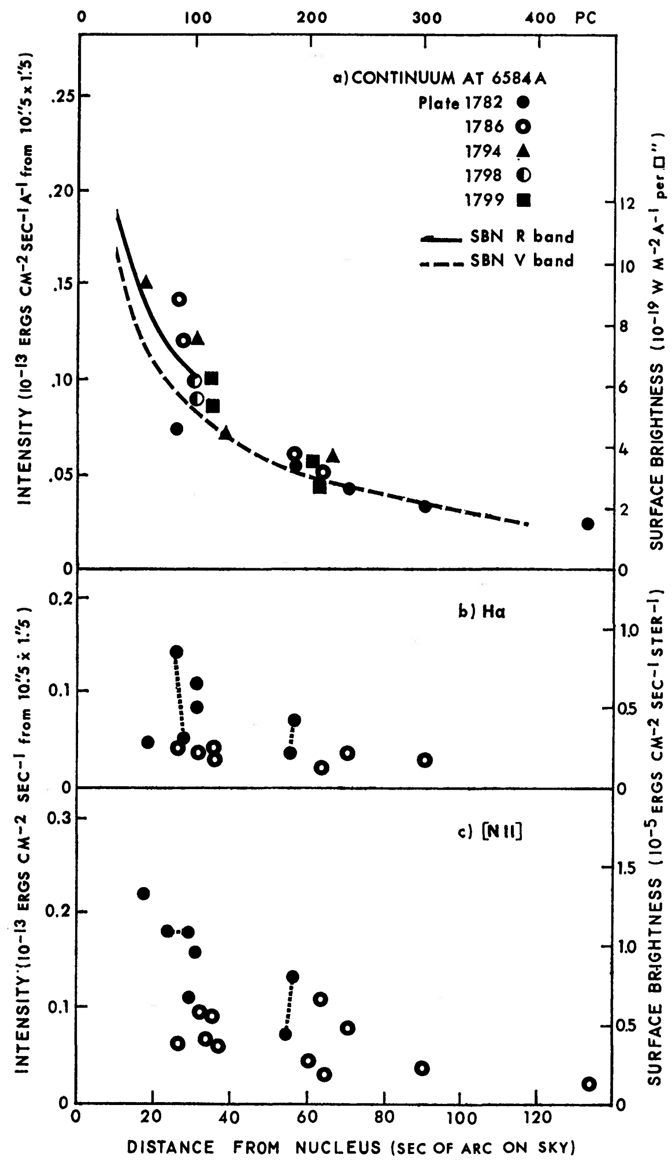

FIG. 9.—(*a*) Absolute intensity and surface brightness of continuum at 6584 Å as a function of distance from nucleus in M31. *Solid line*, surface brightness in *R*-band from Sandage *et al.* (1969). *Dashed line*, surface brightness in *V*-band from Sandage *et al.* (*b*) Absolute intensity and surface brightness in Hα as a function of distance from the nucleus in M31. *Filled circles*, values from dusty regions; *open circles*, values from normal regions. Dashed lines connect values from approximately the same region on different plates. (*c*) Same as Fig. 9*b*, but for [N II] λ6583.

b) Line Intensities

The absolute intensities of the Hα and [N II] λ6583 lines have been measured as a function of radial distance, and the values are listed in Table 5. As can be seen from Figure 1, the emission lines consist generally of narrow continuous emission, but the lines broaden and intensify when the line of sight crosses a dust lane. Values in Table 5 come from either a smooth or a dusty portion of the spectra, and this intensity difference produces much of the scatter shown in Figures 9*b* and 9*c*. The data from plate 1782 are less accurate than data from the other plates, for the spectrum of the nucleus is not contained on the plate; the plate was calibrated by matching the continuum level at 6584 Å to that on plate 1786.

The variation of $I(\mathrm{H}\alpha)$ with radial distance on the sky is plotted in Figure 9*b;* large circles denote dusty regions. There is considerable scatter, mostly real, but a tendency for the Hα intensity to be greater in dusty regions, and to decrease with increasing R. The plot of I([N II]) against R, Figure 9*c*, shows a similar variation. Neither plot is significantly altered if distance in the plane of M31, rather than distance on the sky, is used as the abscissa. For both Hα and [N II], the decrease in intensity is about a factor of 4 in the range $20'' < R < 90''$ (67 pc $< R <$ 300 pc). This is just the factor by which the continuum intensity decreases over this region. Hence, the ratio of emission line to continuum level at 6584 Å, L/C, is constant over this range of radial distance. Individual values of L/C are shown in the final column of Table 5; the mean value is 1.2. As will be discussed below, this is well below the values of L/C for M51 and M81.

The observed flux comes from a region $10\overset{''}{.}5 \times 1\overset{''}{.}52$ on M31, or 7.9×10^{39} cm^2 on the surface of M31 if the inclination of the galaxy is taken into account. Hence, the surface brightness, i.e., the emergent energy at M31, in ergs cm^{-2} s^{-1} sterad^{-1} can be calculated. A scale of surface brightness S is plotted on the right-hand axis of Figures 9*b* and 9*c*. For Hα, the average surface brightness for $R <$ 400 pc is $S \simeq 0.2 \times 10^{-5}$ ergs cm^{-2} s^{-1} sterad^{-1}. For comparison, a bright planetary nebula has a surface brightness of the order of $S = 0.1$ ergs cm^{-2} s^{-1} sterad^{-1} in the [O III] λ5007 line (Aller and Liller 1968). For M31, the total luminosity for a circular area R = 400 pc, over 4π solid angles, is 1×10^{38} ergs s^{-1} in Hα, and twice that in [N II]. Some possible sources of this energy will be discussed in § VI.

c) Nitrogen-to-Hydrogen Ratio

For all radial distances to R = 450 pc (134″), the intensity of [N II] is greater than the Hα intensity, with a mean value for the ratio N/H = 2.2. There is a slight indication that this ratio decreases with radial distance over this small distance. We know from the work of Baade and Arp (1964) that H II regions are not found less than 3 kpc from the nucleus. For the 10 innermost H II regions (3–5 kpc), we have found (Rubin and Ford 1971) that the ratio is $\langle \mathrm{N/H} \rangle = 0.70$. However, five of these regions show strong emission lines; for this group $\langle \mathrm{N/H} \rangle = 1.1$. For all other H II regions in M31, N/H $<$ 1. Hence, the ratio N/H is a slowly decreasing function of radial distance over the nuclear bulge. For distances less than a few hundred parsecs, N/H is greater than 2, and it is just approaching unity in the region where spiral arms containing O and B stars and H II regions are first observed.

d) Comparison with Nuclear Regions of M51, M81, and NGC 4151

For M51 and M81, values for the absolute intensities of Hα and [N II] emission lines near the nucleus, and the continuum at 6584 Å, are available from Peimbert (1968). We have compiled these data in Table 6. The geometry of the emitting regions in M51 and M81 is unknown, so these values refer to face-on observations of spherical emitting regions. Other geometry, i.e., thin disks viewed at some inclination, can introduce factors between 0.5 and 1. From smooth curves drawn through the plots in Figure 9, we have formed absolute intensities for M31 over distances corresponding to those observed in M51 and M81. For the emission lines, I is the intensity received at Earth, corrected for extinction and reddening, per cm^2 per second, over the entire diaphragm. The average surface brightness S is the emergent energy in the emission line, per cm^2 per second per steradian at the galaxy, where S is averaged over the diaphragm size.

Several features emerge from the comparison. Perhaps most noticeable is the difference in L/C, the ratio of line to continuum intensity in the three galaxies. For M81, the average surface brightness in the [N II] line near the nucleus is nearly 100 times that

TABLE 6

COMPARISON OF ABSOLUTE INTENSITIES IN Hα AND [N II] FOR M31, M51, AND M81

Parameter	Diaphragm Radius (pc on Galaxy)	M31	M51	M81
Distance (Mpc)	...	0.69	4.6 (1)	2.5 (1)
Radius (kpc)	...	24 (3)	9.5 (2)	16.8 (2)
Radius of nuclear bulge (kpc)	...	∼2	∼0.3	∼1.5
Mass ($\mathfrak{M}_{\odot}$)	...	1.85×10^{11} (3)	6.4×10^{10} (2)	1.9×10^{11} (2)
Mass/luminosity ($\mathfrak{M}_{\odot}/L_{\odot}$)	...	12 (3)	5.7 (2)	10 (2)
I(Hα)*	0–42	...	...	5.7×10^{-13}
I(Hα)	0–78	2.0×10^{-13}	1.6×10^{-13}	...
I(Hα)	78–223	1.1×10^{-12}	4.3×10^{-13}	...
I(Hα)	0–400	2.5×10^{-12}	...	...
I([N II])	0–42	...	...	8.0×10^{-13}
I([N II])	0–78	3.8×10^{-13}	4.0×10^{-13}	...
I([N II])	78–223	1.8×10^{-12}	4.0×10^{-13}	...
I([N II])	0–400	4.5×10^{-12}	...	...
S(Hα)†	0–42	...	...	6.4×10^{-4}
S(Hα)	0–78	4.9×10^{-4}	1.8×10^{-4}	...
S(Hα)	78–223	3.8×10^{-6}	6.6×10^{-5}	...
S(Hα)	0–400	2.4×10^{-6}	...	...
S([N II])	0–42	...	...	9.0×10^{-4}
S([N II])	0–78	9.4×10^{-6}	4.4×10^{-4}	...
S([N II])	78–223	6.1×10^{-6}	6.2×10^{-5}	...
S([N II])	0–400	4.3×10^{-6}	...	...
I([N II])/I(Hα)	0–42	...	...	1.4
	0–78	2	2.5	...
	78–223	2	0.93	...
	0–400	2	...	...
I(continuum at 6584 Å)‡	0–42	...	...	9.8×10^{-14}
	0–78	2.1×10^{-12}	1.9×10^{-14}	...
	78–223	6.3×10^{-12}	5.8×10^{-14}	...
	0–400	1.7×10^{-11}	...	...
S(continuum at 6584 Å)§	0–42	...	...	1.1×10^{-4}
	0–78	5.2×10^{-5}	2.1×10^{-5}	...
	78–220	2.2×10^{-5}	8.9×10^{-6}	...
	0–400	1.6×10^{-5}	...	...
I([N II])/I(continuum)	0–42	...	...	8.2
	0–78	0.2	21	...
	78–223	0.3	6.9	...
	0–440	0.3	...	...

NOTES.—(1) de Vaucouleurs (1971); (2) Roberts (1969); (3) Rubin and Ford (1970).
* Ergs cm^{-2} s^{-1} received at Earth, corrected for extinction and reddening, from circle or ring of listed radius.
† Ergs cm^{-2} s^{-1} sterad^{-1} emitted at galaxy, averaged over circle or ring of listed radius.
‡ Ergs cm^{-2} s^{-1} Å^{-1}.
§ Ergs cm^{-2} s^{-1} Å^{-1} sterad^{-1}.

in M31, while the continuum levels are more nearly equal. This accounts for the fact that the emission lines in M81 near the nucleus are much easier to detect than in M31. For M51, in the innermost region, the average surface brightness in the [N II] line is about 50 times that in M31, but the average surface brightness in the continuum is down by a factor of about $\frac{1}{2}$ from M31. Hence, the ratio L/C is about 100 times larger in M51 than in M31. In the outer region of the nuclear bulge of M51, the average surface brightness in the [N II] line has decreased while the continuum level has remained more nearly constant, so the ratio L/C has decreased to 20 times that in M31. For the

Seyfert galaxy NGC 4151 (Oke and Sargent 1968), $L/C = 400$ for Hα, and $L/C = 30$ for [N II]. There is thus a fairly regular progression of increasing L/C ratios in spiral galaxies, from less than unity in weak-emission-line galaxies like M31, through strong-emission-line galaxies, up to Seyfert galaxies.

The relative line intensities N/H have also decreased from the inner to the outer nuclear regions of M51, from N/H = 2.5 to N/H = 0.9. Over this region, the average surface brightness in [N II] has decreased by a factor of 7 while the average surface brightness in Hα has decreased by a factor of less than 3. On M51, the outer diaphragm used by Peimbert extended just about to the start of the spiral structure. Thus, just as in M31, in M51 the intensity ratio N/H is greater than 2 near the nucleus, and decreases to unity just at the region where the spiral structure begins, as defined by the O and B stars and the bright H II regions.

For the normal spirals M31, M51, and M81, the energy emitted from the nuclear region in Hα and [N II] is of the order of 10^{38} ergs s^{-1}. In contrast, for NGC 4151 (Oke and Sargent 1968), 25×10^{40} ergs s^{-1} is emitted in Hα, and 1.8×10^{40} ergs s^{-1} is emitted in [N II], over a nucleus assumed to be 50 pc in diameter. Hence, the energy output from this Seyfert galaxy, from emission lines in the nucleus, is over 1000 times that from the nucleus of a normal spiral galaxy like M31.

e) Mass of Ionized Gas and Mass Loss from the Nucleus

Finally, we would like to know the electron density N_e and the mass $\mathfrak{M}$ of the ionized gas near the nucleus of M31. We can estimate the electron density in two ways. First, the ratio of the intensities of the ionized sulfur lines, $I(6731)/I(6717)$, is density dependent. From the calculations of Saraph and Seaton (1970), we estimate that N_e(S II) is of the order of 10^{+4} cm^{-3}, for $I(6731)$ is generally greater than $I(6717)$. In some regions, however, where the intensities of the two lines are comparable, then $N_e(\text{S II}) \leq 10^3$ cm^{-3}.

A second and very different estimate of N_e comes from emission-measure arguments. If the radiation from the gas in the nuclear bulge of M31 comes from an optically thin disk of thickness D pc, with average surface brightness in Hα equal to S per steradian in ergs cm^{-2} s^{-1}, and $T_e = 10{,}000°$, then we write (Aller and Liller 1968):

$$\frac{4\pi S(\mathrm{H}\alpha)}{D'} = N_e^2(2.86 \times 10^{-25}) \text{ ergs cm}^{-3}\text{ s}^{-1}\,,$$

so

$$N_e = \left[\frac{4\pi(0.35 \times 10^{25})S(\mathrm{H}\alpha)}{D'}\right]^{1/2},$$

where D' is the path length in the disk, here assumed to be 100 pc. From Table 6, $S(\mathrm{H}\alpha) = 2.4 \times 10^{-6}$ ergs cm^{-2} s^{-1} sterad^{-1}, averaged over a region out to $R = 400$ pc. Then for the disk of radius 400 pc,

$$N_e(\text{em}) = 0.6 \text{ cm}^{-3}\,.$$

Thus, we see that the average surface brightness in Hα, $S(\mathrm{H}\alpha)$, implies a low density of ionized hydrogen, while the ratio of the [S II] line intensities implies a high density in the emitting regions. If N_e were everywhere as large as the [S II] lines indicate, a very much greater $S(\mathrm{H}\alpha)$ would be observed. Therefore, because $N_e(\text{S II}) \gg N_e(\text{em})$, we are forced to assume that extreme density fluctuations are present in the nuclear region, so that some fraction α of the volume is filled with ionized hydrogen of density N_e(S II) while the remaining volume is empty. To determine the total mass of the disk, we write, following Peimbert (1968),

$$\mathfrak{M}(\text{em}) = \pi r^2 D\, N_e(\text{em})\, m_{\mathrm{H}} = 10^6 \mathfrak{M}_\odot\,,$$

where m_H is the mass of the hydrogen atom,

$$N_e^2(\mathrm{em}) = \alpha N_e^2(\mathrm{S\ II}) ,$$

$$\mathfrak{M}(\alpha) = \pi r^2 D\, N_e(\mathrm{S\ II})\, \alpha m_H = \mathfrak{M}(\mathrm{em})\, \alpha^{1/2} .$$

If $N_e(\mathrm{S\ II}) = 10^4$, then $\alpha = 0.4 \times 10^{-8}$, and $\mathfrak{M}(\alpha) \simeq 100\ \mathfrak{M}_\odot$. Hence, in the extreme high-density model, only a very small fraction of the nuclear region is filled with high-density material, and the total mass of ionized hydrogen is very low. The real value for the mass of ionized matter must lie between the two estimates, $\mathfrak{M}(\mathrm{em})$ and $\mathfrak{M}(\alpha)$.

At either limit, this mass is only an extremely small fraction of the mass located in the nuclear region, which is of the order of $3 \times 10^9\ \mathfrak{M}_\odot$ out to $R = 400$ pc (Rubin and Ford 1970). The mass of neutral hydrogen near the nucleus of M31 is a difficult quantity to determine, because a single 10′ beam of a radio telescope covers 2000 pc along the major axis, 9000 pc along the minor axis. However, from the model studies of Burke, Turner, and Tuve (1964), the total mass out to $R = 400$ pc has a value near $\mathfrak{M}_{\mathrm{H\ I}} = 10^5\ \mathfrak{M}_\odot$. Thus, the mass of neutral hydrogen and the mass of ionized gas in the nuclear bulge of M31, $R \leq 400$ pc, are only a very small fraction of the total mass in this region.

For the model presented above, ionized gas in a disk of radius 400 pc, thickness 25 pc, electron density $N_e = 0.6\ \mathrm{cm}^{-3}$, has a mean velocity radial from the nucleus of about $V = 60\ \mathrm{km\ s}^{-1}$ over 25° of the disk in two directions. This corresponds only to a total mass of $0.01\ \mathfrak{M}_\odot$/year which is leaving the region $R = 400$ pc. Calculations with the gravitational potential in the nuclear region of M31 (R. J. Rubin, unpublished) show that with velocities as low as $100\ \mathrm{km\ s}^{-1}$ the gas will move only hundreds of parsecs, after which it will have lost all of its kinetic energy. Hence, in M31 there is not a large-scale escape of matter from the region $R < 400$ pc. Münch's (1960) original estimate that $1\ \mathfrak{M}_\odot\ \mathrm{year}^{-1}$ was leaving the nucleus of M31 was later decreased (Münch 1962) by a factor of 500. From our observations, it would not be possible to support a value greater than $0.01\ \mathfrak{M}_\odot\ \mathrm{year}^{-1}$ for the mass flow in M31 through the $R = 400$ pc region.

V. COMPARISON WITH THE NUCLEUS OF OUR GALAXY

Only for our own Galaxy and a few others is the angular extent on the sky sufficient to permit a study of details within the nucleus. Thus, it is of interest to compare the distribution and velocities of gas in the nuclei of M31 and our Galaxy.

Early studies by Rougoor and Oort (1960), Rougoor (1964), and most recently by van der Kruit (1970) have led to the following model for neutral hydrogen in the nucleus of our Galaxy. There is a flattened rotating nuclear disk, extending to $R = 750$ pc, with a velocity of $200\ \mathrm{km\ s}^{-1}$ at the edge. At opposite points on the edge of the disk, two arms connect with the 3-kpc arm. These arms may actually form a bar (Kerr 1967). The 3-kpc arm has a radial motion outward from the nucleus, with $V = 53\ \mathrm{km\ s}^{-1}$ where it crosses in front of the nucleus and $V = 135\ \mathrm{km\ s}^{-1}$ where it crosses behind the nucleus. The mass of neutral hydrogen in the nuclear disk is 10^6–$10^7 \mathfrak{M}_\odot$. In the central region, gas is observed outside the plane almost exclusively in two quadrants. The velocities have been interpreted by van der Kruit (1970) as motions outward from the center, arising from an ejection out of the plane from the center in two opposite directions. The sense of the motions, inward or outward, is not uniquely determined by the observations, but is decided by arguments concerning high-velocity clouds and the absence of the features in absorption in front of Sgr A. The mass involved is about $5 \times 10^6\ \mathfrak{M}_\odot$.

In M31, the region $R < 400$ pc would subtend an angle of 6° if observed from a distance of 10 kpc. Over this distance, similarities exist between M31 and our Galaxy. Gas is present in a highly flattened, rapidly rotating disk, with superposed large-scale expansion motions and motions out of the plane. A highly complex pattern of details in the velocity field is seen. The differences which we do observe are minor or not well established: extent of nuclear disk, magnitude of mass leaving the nuclear regions, infall or outgoing motions. The major difference between the two nuclei remains the absence of a nonthermal source in M31, like Sgr A in our Galaxy.

VI. DISCUSSION

We have studied ionized gas in the nuclear bulge of M31, $R \leq 400$ pc, which exhibits a complicated pattern of circular motion, expansion motion, and, in one quadrant, possible infalling motions. At almost every point the velocity dispersion of the gas is small (unlike the velocity dispersion of the stars near the nucleus of M31), which we interpret as indicating that the gas is restricted to a very thin disk. The total energy in the emission lines is 10^{38} ergs s^{-1}; the mass of ionized gas is 10^3–$10^5\ \mathfrak{M}_\odot$. We do not know the source or the mechanism of excitation and ionization of the gas, nor the time-scale dependence of the velocity pattern. The radial motions over path lengths of several hundred parsecs, plus irregularities in the rotation which would smooth out in 10^7 years, imply a time scale of some 10^6 years. The kinetic energy of the gas in the nuclear disk is of the order of 10^{51} ergs; the source of this energy is unknown. We do not know if magnetic fields play a major role.

If an explosion 10^6 or 10^7 years ago generated the outflow of gas, remnants of this explosion could now be falling back to the plane. If the explosion proceeded principally out of the plane, the nuclear disk may have survived the event. If the disk did not survive, then the gas we are now observing could have subsequently re-formed by matter returning to the plane. Explosive phenomena involving large masses and large energies are known for galaxies (M82, NGC 1275), and on smaller scales, for objects like the Crab Nebula.

However, M31 exhibits all of the regularity in structure generally associated with a nonexplosive galaxy, and its nucleus is not an intense radio source. Therefore, a quasi-steady-state model, not involving explosive phenomena, or involving much smaller scale activity, seems more plausible. A most likely source of the gas is mass shed by evolving stars in the nucleus. Arny (1970), following Deutsch (1960), has shown that gas will collect in the nuclei of galaxies. For a nucleus of 10^8 K giants, a mass of $10^6\ \mathfrak{M}_\odot$ would collect in 10^6 years. It seems likely that for a flattened spiral system the gas could form in a thin disk (Rougoor and Oort 1960; Peebles, private communication). Thus the gas we observe falling to the disk could be the source of the gas which forms the disk. Because most of the gas is probably neutral and because we observe only the excited gas, it is not possible to give a meaningful estimate of the mass of the infalling material, from our observations. Given a cloud of mass 100 $\mathfrak{M}_\odot$, with a mean infall velocity of 100 km s^{-1} from a height of 25 pc, then $10^{-3}\ \mathfrak{M}_\odot$ year^{-1} will reach the plane.

Additional evidence that the gas has collected from evolving stars comes from the nitrogen/hydrogen ratio. For gas in the nuclear disk of M31, the intensity of [N II] is twice that of Hα. Hence, the abundance of nitrogen relative to hydrogen may be greater than the solar abundance, as Peimbert (1968) has observed in the nuclei of M51 and M81. This overabundance of nitrogen relative to hydrogen could arise because the gas has been processed through a generation of stars (see discussion in Tammann 1970), making it unlikely that we are observing primordial gas left over from the formation of M31.

Although in this paper we have discussed the disk of gas only to $R = 400$ pc, we have observed the [N II] λ6584 emission line at lower dispersion out to $R = 4$ kpc (Paper I), well in the region at which normal H II regions are observed. In M33 also, Carranza *et al.* (1968) observed a diffuse Hα disk out to $R = 9'$ (1800 pc) which they could distinguish from emission from conventional H II regions. In the disk (as opposed to the arms), Hα was generally half as intense as [N II]. From these observations we infer that disks of low-excitation gas existing in the nucleus and between the arms may not be a rare phenomenon in spiral galaxies.

The source of excitation is unknown. The excitation could come from a fraction of the energy of supernovae (novae would not be sufficient), or a small number of young stars, perhaps newly forming from the gas, or blue-horizontal-branch stars as postulated by Minkowski and Osterbrock (1959) for the excitation of gas in nuclei of elliptical galaxies, or nuclei of planetary nebulae (Hills 1971), or a low flux of high-energy particles, or the passage of stars at supersonic velocities, or none of these. Whatever the mechanism, it may also be responsible for the upturn in the spectrum in the nuclear region of M31 below 2700 Å (Code 1969).

From recent theoretical studies of nuclei, two models have been advanced which may be of significance for our observations. (1) From studies of small-amplitude density waves on a flat galaxy, Kalnajs (1970) has shown that the density wave is essentially a barlike distortion in the central region which drives the gas. In M31 the radial expansion along a bar in position angles 180° apart is a very prominent feature in the velocity field in the nuclear disk. (2) Spiegel (1970) and Moore and Spiegel (1968) have suggested a steady-state model for the flux of gas in the nucleus of our Galaxy. An outflow of gas from the nucleus is arrested near $R = 3$ kpc by a complicated shock, ionizing the gas and lifting much of it outside the galactic plane. For our Galaxy, the shock is identified with the 3-kpc expanding arm. The gas out of the plane falls in toward the nucleus, replenishing the gas supply. We may be observing some effects of a similar pattern in M31.

Clearly, there are many questions unanswered in the present study. Highly complex phenomena which we can only partly understand are taking place in the nucleus of the normal spiral galaxy M31. Additional detailed studies will be necessary to indicate how to relate this nuclear activity to that observed in even more complex and explosive galaxies.

We wish to thank Dr. J. S. Hall, Director of the Lowell Observatory, and Dr. N. U. Mayall, Director of the Kitt Peak National Observatory, for making telescope time available, and Miss Henrietta Swope and W. C. Miller for selecting and copying Baade's plates of the nuclear region of M31. We also thank numerous colleagues for valuable discussions, especially Dr. Krishna Kumar for aid with the spectrophotometric discussion, Dr. Sidney van den Bergh for photographs of the nuclear region of M31, Dr. Robert J. Rubin, Dr. Morton Roberts, and Mrs. Sandra Faber.

APPENDIX

RELATION BETWEEN PLANE OF SKY AND PLANE OF M31 FOR $\xi = 77°$

Position-Angle Plane of Sky (degrees)	Position-Angle Plane of M31 (degrees)	Seconds of Arc in M31 for 1 Sec on Sky	Position-Angle Plane of Sky (degrees)	Position-Angle Plane of M31 (degrees)	Seconds of Arc in M31 for 1 Sec on Sky
38	0	1.0	218	180	1.0
45	29	1.1	225	209	1.1
68	69	2.4	248	249	2.4
98	83	3.9	278	263	3.9
128	90	4.4	308	270	4.4
158	97	3.9	338	277	3.9
188	111	2.4	8	291	2.4
212	154	1.1	32	331	1.1

REFERENCES

Aller, L. H., and Liller, W. 1968, in *Nebulae and Interstellar Matter*, ed. B. M. Middlehurst and L. H. Aller (Chicago: University of Chicago Press), p. 483.
Arny, T. T. 1970, *M.N.R.A.S.*, **148**, 63.
Baade, W., and Arp, H. 1964, *Ap. J.*, **139**, 1027.
Babcock, H. W. 1939, *Lick Obs. Bull.*, No. **498**, 41.
Burke, B. F., Turner, K. C., and Tuve, M. A. 1964, *Carnegie Yrb.*, **63**, 341.
Carranza, G., Courtes, G., Georgelin, Y., Monnet, G., and Pourcelot, A. 1968, *Ann. d'ap.*, **31**, 63.
Code, A. D. 1969, *Pub. A.S.P.*, **81**, 475.
Deutsch, A. J. 1960, in *Stellar Atmospheres*, ed. J. L. Greenstein (Chicago: University of Chicago Press), p. 543.
Hills, J. G. 1971, *Astr. and Ap.* (in press).
Johnson, H. M. 1961, *Ap. J.*, **133**, 309.
Kalnajs, A. J. 1970, in *The Spiral Structure of Our Galaxy*, ed. W. Becker and G. Contopoulos (New York: Springer-Verlag), p. 318.
Kerr, F. J. 1967, in *Radio Astronomy and the Galactic System*, ed. H. van Woerden (London and New York: Academic Press), p. 239.
Lallemand, A., Duchesne, M., and Walker, M. F. 1960, *Pub. A.S.P.*, **72**, 76.
Lyngå, G. 1959, *Medd. Lund Astr. Obs.*, Ser II, No. 137.
Minkowski, R., and Osterbrock, D. 1959, *Ap. J.*, **129**, 583.
Moore, D. W., and Spiegel, E. A. 1968, *Ap. J.*, **154**, 863.
Münch, G. 1960, *Ap. J.*, **131**, 250.
———. 1962, in *Problems of Extra-Galactic Research*, ed. G. C. McVittie (New York: Macmillan Co.), p. 119.
Oke, J. B., and Sargent, L. W. 1968, *Ap. J.*, **151**, 807.
Peimbert, M. 1968, *Ap. J.*, **154**, 33.
Roberts, M. S. 1969, *A.J.*, **74**, 859.
Rougoor, G. W. 1964, *B.A.N.*, **17**, 381.
Rougoor, G. W., and Oort, J. H. 1960, *Proc. Nat. Acad. Sci.*, **46**, 1.
Rubin, V. C., and Ford, W. K., Jr. 1970, *Ap. J.*, **159**, 379 (Paper I).
———. 1971, in *External Galaxies and Quasi-stellar Objects* (in press).
Sandage, A. R., Becklin, E. E., and Neugebauer, G. 1969, *Ap. J.*, **157**, 55.
Saraph, H. E., and Seaton, M. J. 1970, *M.N.R.A.S.*, **148**, 367.
Scheiner, J. 1899, *Ap. J.*, **9**, 149.
Spiegel, E. A. 1970, I.A.U. Symp. 38, in *The Spiral Structure of Our Galaxy*, ed. W. Becker and G. Contopoulos (New York: Springer-Verlag), p. 441.
Tammann, G. 1970, *Astr. and Ap.*, **8**, 458.
van der Kruit, P. C. 1970, *Astr. and Ap.*, **4**, 467.
Vaucouleurs, G. de. 1971, in *Galaxies and the Universe*, ed. A. and M. Sandage (Chicago: University of Chicago Press) (in press).